Auton Robot (2012) 32:243–266
DOI 10.1007/s10514-011-9270-z

Generalization of the collision cone approach for motion safety in 3-D environments

Animesh Chakravarthy · Debasish Ghose

Received: 22 January 2011 / Accepted: 2 December 2011 / Published online: 22 December 2011

Abstract Avoidance of collision between moving objects in a 3-D environment is fundamental to the problem of planning safe trajectories in dynamic environments. This problem appears in several diverse fields including robotics, air vehicles, underwater vehicles and computer animation. Most of the existing literature on collision prediction assumes objects to be modelled as spheres. While the conservative spherical bounding box is valid in many cases, in many other cases, where objects operate in close proximity, a less conservative approach, that allows objects to be modelled using analytic surfaces that closely mimic the shape of the object, is more desirable. In this paper, a collision cone approach (previously developed only for objects moving on a plane) is used to determine collision between objects, moving in 3-D space, whose shapes can be modelled by general quadric surfaces. Exact collision conditions for such quadric surfaces are obtained and used to derive dynamic inversion based avoidance strategies.

Keywords Collision cone · Dynamic environments · Obstacle avoidance · Path planning · Quadric surfaces

A. Chakravarthy (✉)
Department of Aerospace Engineering and the Department of Electrical Engineering, Wichita State University, Wichita, KS 67260, USA
e-mail: animesh.chakravarthy@wichita.edu

D. Ghose
Guidance, Control and Decision Systems Laboratory (GCDSL) in the Department of Aerospace Engineering, Indian Institute of Science, Bangalore, India
e-mail: dghose@aero.iisc.ernet.in

1 Introduction

An important component of robot path planning is the obstacle avoidance problem, that is, determining a safe trajectory of a robotic vehicle so that it circumvents various stationary as well as dynamic obstacles of arbitrary shapes. A commonly used metric for many path planning algorithms is obstacle complexity, or the amount of information used to store a computer model of the obstacle (Kim et al. 2006). Obstacle complexity can be measured in terms of the number of obstacle edges (Goerzen et al. 2010). A common practice then is to use a bounding box approximation for the objects. The obstacle avoidance conditions are then computed for the bounding box as a whole—this is as opposed to performing a spatial discretization of the object and then computing avoidance conditions for each such discrete component separately. In particular, generation of analytical expressions that give collision avoidance conditions for such bounding boxes are particularly helpful, since they can lead to tremendous computational savings, especially in multi-obstacle environments.

The choice of a bounding box involves the inherent trade-off that exists between computational ease and accuracy/precision and also must account for the dimension of the physical space. In the 2-D case, even when the object is of arbitrary shape, a circular bounding box has both perfect precision/accuracy as well as analytical form Chakravarthy and Ghose (1998). In 3-D this no longer holds and a straightforward extension to spherical bounding surface can only be analytical but it cannot satisfy the requirement of precision to a satisfactory level. This is especially true when objects are expected to move in close proximity to each other. Thus, while spheres do serve as common bounding box approximations for many objects in space (because of the computational ease associated with them), these approximations

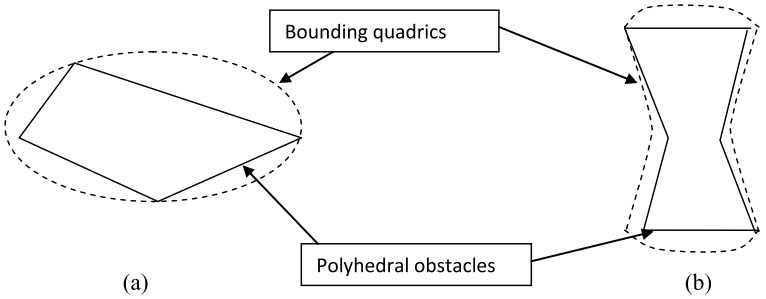

Fig. 1 Examples of polyhedral obstacles wherein the use of a spherical bounding box approximation can be overly conservative. In (**a**), an ellipsoid serves as a better bounding box while in (**b**), a confocal quadric is used

can become overly conservative in cases when an object is more elongated along one dimension compared to the other (as shown in Fig. 1(a), for example). In such cases, a non-spherical object such as an ellipsoid or a spheroid can serve as a better approximation for the object (Ju et al. 2001; Choi et al. 2006, 2009). The fuselage of an aeroplane or a submarine are also instances where an ellipsoid can serve as a better bounding box than a sphere. There can, however, be cases when even ellipsoids turn out to be overly conservative—this is particularly true if they are used to approximate certain objects of non-convex cross-section. In such cases, a hyperboloid can be a potential candidate for approximation purposes (since a hyperboloid is essentially non-convex). Hyperboloids by themselves are of infinite size, but when used in conjunction with a spheroid or an ellipsoid (which are convex but of finite size), they can be used to approximate non-convex objects of finite size. Indeed, the intersection of a hyperboloid with a spheroid would be one such example of a non-convex finite sized object that can be used for such bounding box approximation purposes (as shown in Fig. 1(b), for example). Such an approximation would also be suitable for a micro air vehicle with bat-like wings.

Spheres, ellipsoids, spheroids, hyperboloids all fall into the broad category of quadric surfaces. Quadric surfaces can be used to form more precise bounding box approximations. Additionally, suitable combinations of such quadric surfaces can be used to approximate an even larger class of objects. Determination of analytical representations of collision avoidance conditions for quadric surfaces is therefore a relevant topic of study. In three dimensional space, a quadric surface (Hilbert and Cohn-Vossen 1952) is defined as one that can be represented by an equation of the general form:

$$Ax^2 + By^2 + Cz^2 + Dxy + Eyz + Fxz + Gx + Hy + Kz + L = 0 \quad (1)$$

In this paper, we obtain fairly general collision and avoidance conditions for quadric surfaces. We start from basic collision conditions between two point objects. The earliest works on studying collision conditions between point objects came from the missile guidance literature (Zarchan 1990; Shneydor 1998; Lin 1991) in which the collision conditions were used to develop empirical guidance laws such as proportional navigation and constant bearing course guidance. However, due to the very restrictive nature of the point mass object assumption, these results had rather limited applications in the robotics community. Subsequently, two independently developed approaches of velocity obstacles (Fiorini and Shiller 1998) and collision cones (Chakravarthy and Ghose 1998) appeared. Both considered rectilinear motion of objects (say, A and B) on a plane and obtained conditions under which a collision between them occurs. The velocity obstacles method (Fiorini and Shiller 1998) defined a set of points in the planar configuration space of A, such that if any velocity vector of object A (in terms of *both* magnitude and direction) lies in this set then collision occurs. This set is called a velocity obstacle. This method considers only circular objects and reduces the problem to the configuration space (Lozano-Perez 1983) of object A by enlarging object B and reducing object A to a point. Generalization to arbitrarily shaped objects are not considered. However, in later papers (Shiller et al. 2001; Large et al. 2005), the velocity obstacle method was extended to obstacles with curvilinear paths. The collision cone approach (Chakravarthy and Ghose 1998), on the other hand, considered the velocity of one of the objects (say, B) to be fixed and determined the cone of directions of the velocity of object A (with only its magnitude fixed) for which it collides with object B. This cone was termed as the *collision cone*. This notion of collision cone was used to generalize and obtain collision conditions even when the objects were of arbitrary shapes. This approach thus yielded a closed-form representation of the collision conditions, for objects of arbitrary shapes moving on a plane. The advantage of obtaining such exact analytical expressions for collision cones lies in the fact that these expressions can then serve as an efficient platform for the analysis and computation of provably safe trajectories.

The collision cone method introduced in Chakravarthy and Ghose (1998) has been used extensively in several papers, for example: Ferrara and Vecchio (2007, 2009), Ferrara and Paderno (2006), Ferrara and Rubagotti (2007), Watanabe et al. (2006a, 2006b, 2007a, 2007b), Carbone et al. (2006), Gross et al. (2004), and Lalish and Morgansen (2008). In Ferrara and Vecchio (2007, 2009) and Ferrara and Paderno (2006), the collision cone method was used in the

context of car collision avoidance to develop a driver assistance system. In Ferrara and Rubagotti (2007), the collision cone approach (Chakravarthy and Ghose 1998) was combined with the potential field approach (Khatib 1986) to guide a mobile robot toward its goal, while safely avoiding the obstacles. In Watanabe et al. (2006a, 2006b, 2007a, 2007b), Carbone et al. (2006), and Gross et al. (2004), the collision cone concept was used in the context of safe trajectories for aircraft, while in Lalish and Morgansen (2008) it was used in the context of an n-vehicle collision avoidance problem.

The extension to collision between two objects in the three-dimensional space, which is of greater practical importance due to the inherent three-dimensional nature of collision avoidance problems in robotics or close proximity operations of MAVs (micro air vehicles), is not straightforward, except perhaps in the case when the objects are modeled as spheres. In fact, the papers cited above, that use the collision cone concept in 3-D (for instance, Watanabe et al. 2006a, 2006b, 2007a, 2007b; Carbone et al. 2006; Gross et al. 2004), as also other papers that discuss collision in 3-D (such as Belkouche 2009; Bendjilali and Belkhouche 2009), apply the notion of collision cone in 3-D space but use the basic 2-D results or make strong assumptions about the objects being spherical. The collision cone concept introduced in Chakravarthy and Ghose (1998) used the relative velocity framework, popular in the aerospace guidance literature (for instance, see Chakravarthy and Ghose 1996; Guelman 1976; Tyan 2005) quite extensively. Further work in the relative velocity framework on the performance of guidance laws through capturability conditions, produced extensions of these notions to 3-D geometries where the relative velocity framework was extended to a modified polar coordinate system which reduced the number of differential equations needed to describe the relative dynamics (Tyan 2005). However, the work in Tyan (2005) confined itself to point mass models for the objects. In the present paper, we continue to use the relative velocity framework proposed in Chakravarthy and Ghose (1998) and obtain fairly general results for analytically obtaining the collision cone for objects represented by quadric surfaces. These represent a fairly large class of objects that can be used to model real-life three dimensional objects like flying, underwater, or robotic vehicles.

This paper is a substantially expanded and detailed version of Chakravarthy and Ghose (2011), where only some preliminary results related to 3-D collision cones with quadric surfaces was presented. The present paper contains extensive results with various classes of quadric surfaces and highlights issues related to guaranteed collision avoidance and motion safety. This paper is organized as follows. Section 2 provides a review of well known collision conditions existing in the aerospace guidance literature concerning two moving point objects in space. Section 3 extends these results to obtain collision conditions between a point and a sphere moving in space; it also demonstrates how these conditions can be used to determine safe trajectories by computing the requisite changes in speed and/or heading required to avoid the sphere by a dynamic inversion technique. Section 4 extends the results of Sect. 2 to get exact analytical expressions governing collision conditions between a point and a spheroid; it also demonstrates the use of these conditions in the determination of safe trajectories that avoid the spheroid. Section 5 discusses collision conditions and safe trajectories between a point and a hyperboloid. Sections 6 and 7 discuss collision cones and safe trajectories for objects of arbitrary shapes, while Sect. 8 discusses the use of collision cones in closed spaces and with multiple obstacles. The paper concludes with Sect. 9 that summarizes the main results and indicates some future directions of research.

2 Basic collision results

The engagement geometry for an interception problem between two point objects A and B is shown in Fig. 2. Note that the line-of-sight (LOS) vector between A and B is defined by the pair of angles (θ, ϕ), where θ and ϕ represent the azimuth and elevation angles, respectively. Similarly, the velocity vectors for $\vec{V}_A$ and $\vec{V}_B$ are defined by the angle pairs (β, α) and (μ, η), respectively which are the azimuth and elevation angle pairs for these vectors. (These angles are not shown in Fig. 2.) We thus have

$$\vec{V}_A = V_A(\cos\alpha\cos\beta\,\vec{i} + \cos\alpha\sin\beta\,\vec{j} + \sin\alpha\,\vec{k}) \tag{2}$$

$$\vec{V}_B = V_B(\cos\eta\cos\mu\,\vec{i} + \cos\eta\sin\mu\,\vec{j} + \sin\eta\,\vec{k}) \tag{3}$$

$$\begin{aligned}\vec{V}_{AB} = \vec{V}_B - \vec{V}_A &= (V_B\cos\eta\cos\mu - V_A\cos\alpha\cos\beta)\,\vec{i} \\ &\quad + (V_B\cos\eta\sin\mu - V_A\cos\alpha\sin\beta)\,\vec{j} \\ &\quad + (V_B\sin\eta - V_A\sin\alpha)\,\vec{k}\end{aligned} \tag{4}$$

In (4), $\vec{V}_{AB}$ is the relative velocity of B with respect to A, and characterizes the motion of the LOS in space. In order

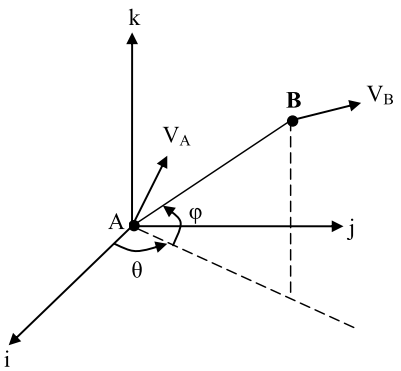

Fig. 2 Engagement geometry between two point objects

to represent the components of the LOS in a spherical coordinate frame, first rotate the original frame of reference by θ about the $\vec{k}$ axis and then rotate the resulting frame about the new $\vec{j}$ axis by ϕ. In this new reference frame, the component of the relative velocity along the new $\vec{i}$ axis is denoted by V_r, its component along the new $\vec{j}$ axis is denoted by V_θ, and its component along the new $\vec{k}$ axis is denoted by V_ϕ. Thus, V_r is the component of the relative velocity along the LOS and the resultant of V_θ and V_ϕ represents the component normal to the LOS. Obviously they satisfy,

$$V_\theta^2 + V_\phi^2 + V_r^2 = V_{AB}^2 \tag{5}$$

The rotational transformations described above yield the following relations,

$$V_\theta = r\dot{\theta}\cos\phi = V_B\cos\eta\sin(\mu-\theta) - V_A\cos\alpha\sin(\beta-\theta) \tag{6}$$

$$V_\phi = r\dot{\phi} = V_B\{-\cos\eta\sin\phi\cos(\mu-\theta) + \sin\eta\cos\phi\} - V_A\{-\cos\alpha\sin\phi\cos(\beta-\theta) + \sin\alpha\cos\phi\} \tag{7}$$

$$V_r = \dot{r} = V_B\{\cos\eta\cos\phi\cos(\mu-\theta) + \sin\eta\sin\phi\} - V_A\{\cos\alpha\cos\phi\cos(\beta-\theta) + \sin\alpha\sin\phi\} \tag{8}$$

Assuming $\vec{V}_A$ and $\vec{V}_B$ to be constants and differentiating the relative velocity components, we obtain,

$$\begin{aligned}\dot{V}_\theta &= -\dot{\theta}(V_r\cos\phi - V_\phi\sin\phi)\\ \dot{V}_\phi &= -\dot{\phi}V_r - \dot{\theta}V_\theta\sin\phi\\ \dot{V}_r &= \dot{\phi}V_\phi + \dot{\theta}V_\theta\cos\phi\end{aligned} \tag{9}$$

Eliminating $\dot{\theta}$ and $\dot{\phi}$ from the above equations we get,

$$\dot{V}_\theta V_\theta + \dot{V}_\phi V_\phi + \dot{V}_r V_r = 0 \tag{10}$$

which on integration yields,

$$V_\theta^2 + V_\phi^2 + V_r^2 = V_{\theta0}^2 + V_{\phi0}^2 + V_{r0}^2 \tag{11}$$

where, the subscript '0' indicates the values of the relative velocity components at some initial time $t = t_0$. Equation (11) shows that the time trajectory of the LOS in the (V_θ, V_ϕ, V_r)-space lies on the surface of a sphere with centre at the origin and radius equal to the magnitude of the relative velocity between A and B. We can gain additional information of the time evolution of these trajectories as follows:

Multiplying r on both sides of each of (9) and using (6)–(8) we obtain,

$$\begin{aligned}r\dot{V}_\theta &= -V_\theta V_r + V_\phi V_\theta\tan\phi\\ r\dot{V}_\phi &= -V_\phi V_r - V_\theta^2\tan\phi\\ r\dot{V}_r &= V_\theta^2 + V_\phi^2\end{aligned} \tag{12}$$

Since the right hand side of the last equation in (12) is always positive, and also $r > 0$, we can infer that $\dot{V}_r > 0$, that is, the trajectories everywhere on the surface of the sphere defined by (11) always move along the direction of increasing V_r. We can now state the following lemmas generalized to three-dimensional space from well-known two-dimensional results available in Chakravarthy and Ghose (1998).

Lemma 1 *Points that satisfy $V_\theta = 0$ and $V_\phi = 0$ are stationary points in the (V_θ, V_ϕ, V_r)-space.*

Proof It is seen from (12), that when $V_\theta = V_\phi = 0$ (and since $r > 0$), we get $\dot{V}_r = \dot{V}_\phi = \dot{V}_\theta = 0$. □

Lemma 2 *If two point objects move with constant velocities, then $V_{\theta0} = 0$, $V_{\phi0} = 0$, and $V_{r0} < 0$, together form a necessary and sufficient condition for collision.*

Proof By Lemma 1, $V_{\theta0} = 0$, $V_{\phi0} = 0$, $V_{r0} < 0$ implies that $V_\theta = 0$, $V_\phi = 0$, $V_r < 0$ for all future time. But $V_\theta = 0$, $V_\phi = 0$ implies that the LOS does not rotate in space and $V_r(= \dot{r}) < 0$ implies that the distance between the two objects is continuously decreasing, thus eventually leading to a collision. This proves sufficiency. The necessity condition can be proved similarly. □

We next look at the trajectories in the (V_θ, V_ϕ, V_r) space.

Case 1: $V_{\theta0} = 0;\ V_{\phi0} = 0;\ V_{r0} < 0$.

In this case, the two point objects A and B are on a collision course (Lemma 2). Also, $(V_{\theta0}, V_{\phi0}, V_{r0})$ is a stationary point on the (V_θ, V_ϕ, V_r)-space (Lemma 1).

Case 2: $V_{\theta0} \neq 0$ and/or $V_{\phi0} \neq 0;\ V_{r0} < 0$.

For Case 2, from (12), a (V_θ, V_ϕ, V_r), trajectory originating from the $V_r < 0$ region, moves into the $V_r > 0$ region since $\dot{V}_r > 0$ always. At the time instant (say, $t = t_m$) when the trajectory penetrates the $V_r = 0$ plane, r is a minimum. Let $r(t_m) = r_m$. Then, from (11), we can infer that

$$V_{\theta m}^2 + V_{\phi m}^2 = V_{r0}^2 + V_{\theta0}^2 + V_{\phi0}^2 \tag{13}$$

where, $V_{\theta m}$ and $V_{\phi m}$ represent $V_\theta(t_m)$ and $V_\phi(t_m)$, respectively. Multiplying V_θ and V_ϕ on both sides of the first two equations of (12), respectively, and adding, we obtain,

$$\frac{V_\theta\dot{V}_\theta + V_\phi\dot{V}_\phi}{V_\theta^2 + V_\phi^2} = -\frac{\dot{r}}{r} \quad\Rightarrow\quad \frac{V_\theta^2 + V_\phi^2}{V_{\theta0}^2 + V_{\phi0}^2} = \left(\frac{r_0}{r}\right)^2 \tag{14}$$

Putting $r = r_m$ at $t = t_m$ and substituting from (13), we get

$$r_m^2 = r_0^2\left(\frac{V_{\theta0}^2 + V_{\phi0}^2}{V_{\theta0}^2 + V_{\phi0}^2 + V_{r0}^2}\right) \tag{15}$$

Equation (15) thus gives the expression for the distance between the point objects A and B at the instant of closest approach as a function of the initial values of the relative velocity components and the initial relative separation.

Note that the expression assumes that the engagement commences at an initial condition $V_{r0} < 0$. If $V_{r0} > 0$, then the same expression gives the distance at closest approach if the trajectories are projected backwards in time. We also note that the time t_m of closest approach is given by

$$t_m = \frac{-r_0 V_{r0}}{(V_{\theta 0}^2 + V_{\phi 0}^2 + V_{r0}^2)} \tag{16}$$

Note that (16) assumes $V_{r0} < 0$ thus leading to positive values of time t_m. In subsequent sections, these results will be used to derive more general collision conditions.

3 Point-sphere collision avoidance

A sphere is obtained from (1) by substituting $A = B = C = 1/R^2$, $D = E = F = G = H = K = 0$ and $L = -1$. We note that collision between a point and a sphere has been presented earlier (for example in Watanabe et al. 2007a; Carbone et al. 2006; Gross et al. 2004; Frazzoli et al. 2001) in several alternative forms. However, we will show that presenting the conditions in the relative velocity framework (as is done in Sect. 3.1) allows us to subsequently use the notion of collision cone equivalence and thereby obtain both collision conditions as well as avoidance maneuvers between a point and an additional class of objects.

3.1 Exact conditions for collision

Refer to Fig. 3, where A is a point object, and $\mathcal{F}$ is a sphere of radius R with center at P. AP is defined as the LOS—its angular orientation and velocity vectors are as in the previous section.

Lemma 3 *If a point object A and a sphere $\mathcal{F}$ move with constant velocities, then A is on a collision course with $\mathcal{F}$ if and only if there exists a ray AC, passing through $\mathcal{F}$, for which $(V_\theta)_{AC} = 0$; $(V_\phi)_{AC} = 0$; $(V_r)_{AC} < 0$ (C is then the point of collision).*

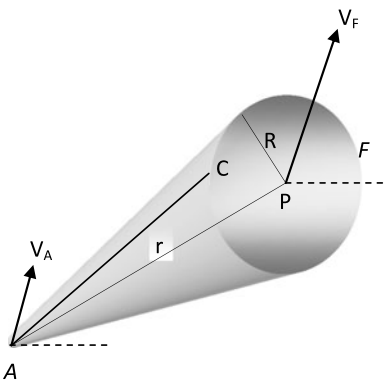

Fig. 3 Collision geometry between a point and a sphere

Proof Follows from Lemma 2. □

In (15), let V_{r0}, $V_{\theta 0}$, and $V_{\phi 0}$ represent the initial relative velocity components of the line AP. It is then easy to see that A colliding with any point on $\mathcal{F}$ is described by the condition $r_m \leq R$. Implementing this condition in using (15), we get

$$r_0^2(V_{\theta 0}^2 + V_{\phi 0}^2) \leq R^2(V_{\theta 0}^2 + V_{\phi 0}^2 + V_{r0}^2)$$
$$V_{r0} < 0 \tag{17}$$

Thus if a point and a sphere move with constant velocities with initial conditions that satisfy (17) then they are headed for a collision. These conditions are both necessary and sufficient for a collision to occur.

Putting $R = 0$ in (17) reduces it to $V_{\theta 0} = 0$, $V_{\phi 0} = 0$, and $V_{r0} < 0$, which are the conditions for collision between two point objects (Lemma 2).

Substituting $V_{\theta 0}$, $V_{\phi 0}$ and V_{r0}, from (6)–(8), in (17), we get two inequalities in terms of θ_0, ϕ_0, r_0, V_A, V_B, α , β, η, μ and R. Then, there exists a range of α and β that satisfies these inequalities. Thus, every (β, α) pair that satisfies (17) will lead to a collision with B. Note that each (β, α) pair denotes a unit vector direction. The collection of these unit vectors, all originating from A, forms the *collision cone* with its vertex at A.

Lemma 4 *If a point and a sphere of radius R move with constant velocities and initial conditions that satisfy* (17)*, then they will continue to satisfy the condition $r^2(V_\theta^2 + V_\phi^2) \leq R^2(V_\theta^2 + V_\phi^2 + V_r^2)$ for all future time.*

Proof Define a function $y(t)$ as,

$$y(t) = r^2(V_\theta^2 + V_\phi^2)/(V_\theta^2 + V_\phi^2 + V_r^2) - R^2 \tag{18}$$

Differentiating (18) with respect to t, and substituting (10) and (14) we get $dy(t)/dt = 0$, which implies that the value of $y(t)$ remains constant. Thus, if $y(t) < 0$ initially, it remains so for all future time. □

Lemma 4 is thus a generalization of Lemma 1.

We point out that in the computation of $y(t)$ using (18), measurements of $V_\theta(t)$, $V_\phi(t)$, $V_r(t)$ and $r(t)$ are required. Depending on the type of sensors used, these quantities can either be obtained as measurements directly from the sensors, or they may be obtained using nonlinear estimation methods that convert measurements of other sensed quantities into V_θ, V_ϕ, V_r and r. The determination of a good update rate depends on how rapidly the vehicles in the specific environment under consideration, are maneuvering. In this paper, we present the avoidance techniques in a general framework that does not restrict itself to a single specific application or sensor type.

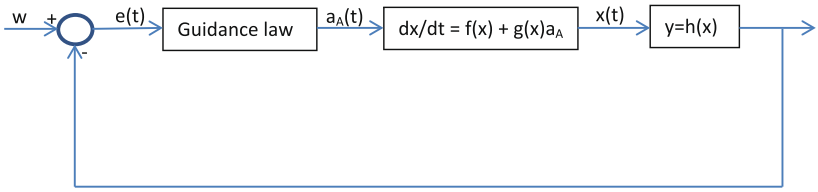

Fig. 4 Block diagram for dynamic inversion-based avoidance maneuver design

3.2 Collision avoidance

From (18), an analytical expression for a guidance law for collision avoidance can be determined using a nonlinear dynamic inversion technique (Slotine and Li 1991) in the form shown in Fig. 4. Collision avoidance is ensured by driving $y(t)$ to zero. This is seen as follows: for any trajectory, at the point of closest approach, $V_r = 0$ holds. This is true irrespective of whether object A and/or B is accelerating or not. Then, substituting $V_r = 0$ in (18), we see that $y(t) = 0$ if and only if $r(t) = R$.

The state equation, $\dot{x} = f(x) + g(x)u$ is of the form:

$$\begin{bmatrix} \dot{r} \\ \dot{\theta} \\ \dot{\phi} \\ \dot{V}_\theta \\ \dot{V}_\phi \\ \dot{V}_r \end{bmatrix} = \begin{bmatrix} V_r \\ V_\theta/(r\cos\phi) \\ V_\phi/r \\ (-V_\theta V_r + V_\theta V_\phi \tan\phi)/r \\ (-V_\phi V_r - V_\theta^2 \tan\phi)/r \\ (V_\phi^2 + V_\theta^2)/r \end{bmatrix} + \begin{bmatrix} 0 \\ 0 \\ 0 \\ -\cos\gamma \sin(\delta-\theta) \\ \cos\gamma \sin\phi \cos(\delta-\theta) - \sin\gamma\cos\phi \\ -\cos\gamma\cos\phi\cos(\delta-\theta) - \sin\gamma\sin\phi \end{bmatrix} a_A \tag{19}$$

In (19), a_A is the acceleration of the point object A, which is applied at an azimuth angle δ and an elevation angle γ. This equation is affine in the input a_A. γ and δ are defined a priori and may or not be constants. It is noted that if either r or $\cos\phi$ become zero, then some states in (19) become unbounded. However, since $r \geq R$, it can never become zero. When $\cos\phi$ becomes zero, then the engagement geometry is two-dimensional and this can be readily handled by reducing the state vector to comprise of only r, ϕ, V_ϕ, V_r. Now, the output equation $y = h(x)$ has the form of (18), and since $\dot{y} = \frac{\partial y}{\partial x}\dot{x}$

$$\dot{y} = \begin{bmatrix} \frac{\partial y}{\partial r} & \frac{\partial y}{\partial \theta} & \frac{\partial y}{\partial \phi} & \frac{\partial y}{\partial V_\theta} & \frac{\partial y}{\partial V_\phi} & \frac{\partial y}{\partial V_r} \end{bmatrix} \times \begin{bmatrix} \dot{r} & \dot{\theta} & \dot{\phi} & \dot{V}_\theta & \dot{V}_\phi & \dot{V}_r \end{bmatrix}^T \tag{20}$$

The vector $\frac{\partial y}{\partial x}$ as obtained from (18) has the elements:

$$\begin{aligned} &\frac{\partial y}{\partial r} = 2r(V_\theta^2 + V_\phi^2)/(V_\theta^2 + V_\phi^2 + V_r^2); \qquad \frac{\partial y}{\partial \theta} = 0 \\ &\frac{\partial y}{\partial \phi} = 0; \qquad \frac{\partial y}{\partial V_\theta} = 2r^2 V_\theta V_r^2/(V_\theta^2 + V_\phi^2 + V_r^2)^2 \\ &\frac{\partial y}{\partial V_\phi} = 2r^2 V_\phi V_r^2/(V_\theta^2 + V_\phi^2 + V_r^2)^2 \\ &\frac{\partial y}{\partial V_r} = -2r^2 V_r(V_\theta^2 + V_\phi^2)/(V_\theta^2 + V_\phi^2 + V_r^2)^2 \end{aligned} \tag{21}$$

Substituting (21) and (19) in (20), and simplifying we get

$$\begin{aligned} a_A = (0.5\dot{y}/r^2)(V_\theta^2 + V_\phi^2 + V_r^2)^2/[&-V_\theta V_r^2 \cos\gamma \sin(\delta-\theta) \\ &+ V_\phi V_r^2\{\cos\gamma\sin\phi\cos(\delta-\theta) - \sin\gamma\cos\phi\} \\ &+ V_r(V_\theta^2 + V_\phi^2)\{\cos\gamma\cos\phi\cos(\delta-\theta) + \sin\gamma\sin\phi\}] \end{aligned} \tag{22}$$

Next, define an error signal $e(t) = w(t) - y(t)$, where $w(t)$ is the reference input indicated in Fig. 4. Thus, $\dot{y} = \dot{w} - \dot{e}$. Taking $w(t) = 0\ \forall t$ and enforcing the error dynamics to be $\dot{e} = -Ke$, (with $K > 0$), we get $\dot{y} = Ke = -Ky$. Substitute this in (22) to obtain:

$$\begin{aligned} a_A = (-0.5K(V_\theta^2 + V_\phi^2 + V_r^2)/r^2)[&r^2(V_\theta^2 + V_\phi^2) \\ &- R^2(V_\theta^2 + V_\phi^2 + V_r^2)]/[-V_\theta V_r^2\cos\gamma\sin(\delta-\theta) \\ &+ V_\phi V_r^2\{\cos\gamma\sin\phi\cos(\delta-\theta) - \sin\gamma\cos\phi\} \\ &+ V_r(V_\theta^2 + V_\phi^2)\{\cos\gamma\cos\phi\cos(\delta-\theta) \\ &+ \sin\gamma\sin\phi\}] \end{aligned} \tag{23}$$

Equation (23) is a guidance law that will drive $y(t)$ to zero. Note that since the error dynamics $e(t)$ are first order, therefore any positive value of K will guarantee that $y(t)$ exponentially decays to zero. Further, when $y(t)$ becomes zero it corresponds to the physical scenario of the velocity vector of A being aligned with the boundary of the collision cone. Now in theory, the exponential nature of $y(t)$ will mean that $y(t)$ goes to zero only as $t \to \infty$. However, if the original radius of the sphere R is increased to $R + \epsilon$, where $\epsilon > 0$ is a small number, it can be ensured that $y(t)$ corresponding to R will go to zero in finite time, as $y(t)$ corresponding to $R + \epsilon$ goes to zero asymptotically.

We however need to choose K to be at least as large as to ensure that $y(t)$ decays to zero before the time t_m defined in (16). The error dynamics equation has a solution of the form: $e(t) = e(0)e^{-Kt}$, where $e(0)$ indicates the initial error. We require this error decays to ϵ within a time less than t_m. It can be seen that this would be ensured by choosing

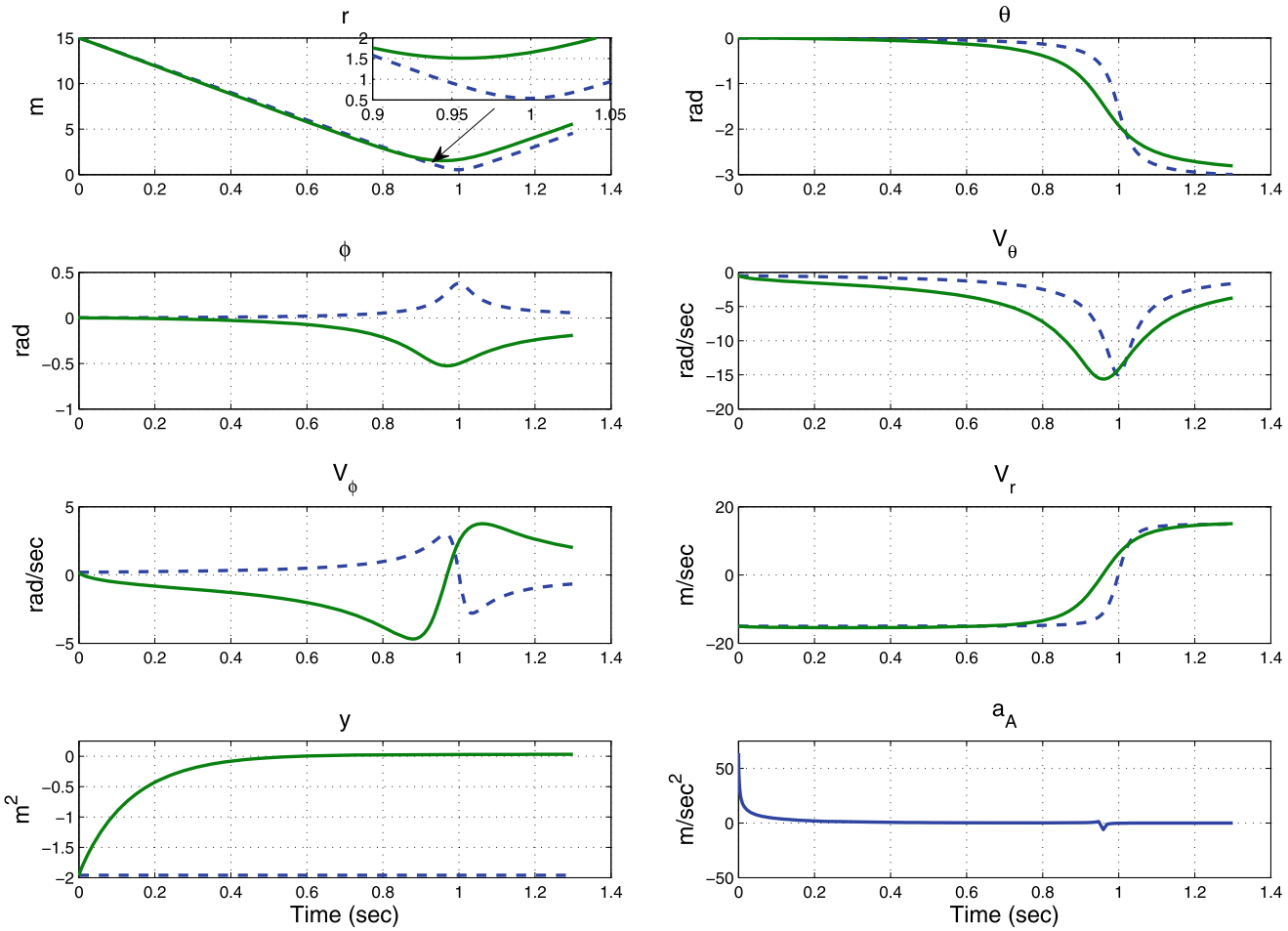

Fig. 5 State, input and output trajectories in open loop (- - -) and closed loop (—) in a point-sphere engagement

a K that satisfies $K > \frac{1}{t_m} \ln(\frac{e(0)}{\epsilon})$, (wherein it is understood that $\epsilon < e(0)$). An upper bound on K would be fixed by the acceleration limits of the vehicle.

These results lead to the following theorem.

Theorem 1 *If a point and a sphere are moving such that at $t = t_0$, the velocity vector of the point lies inside the collision cone (17), then if the point uses the acceleration law given in (23), its velocity vector will leave the collision cone at some time $t_1 \in [t_0, t_m]$. If the sphere moves with constant velocity for all $t \geq t_0$ and the point moves with constant velocity for all $t \geq t_1$, collision avoidance is guaranteed.*

Proof Follows from the analysis given above. □

We point out that there can be situations when the denominator term in (23) becomes zero. Since all physical systems have a limit on their acceleration capabilities, this would correspond to the acceleration limit of the system being reached. The robotic vehicle then has the option of either applying the maximum acceleration, or explore if there is an alternative (δ, γ) pair that will make the denominator non-zero. In a multi-obstacle scenario, an optimal choice of (δ, γ) would be determined by the relative trajectories of the different obstacles, i.e. the direction of the applied acceleration should be such that in trying to avoid one obstacle, a collision with a different obstacle should not occur. Such aspects regarding the appropriate choice of (δ, γ) remain avenues for further research and are outside the scope of the current paper.

Example 1 Consider a point and a sphere of radius $R = 1.5$, moving with initial conditions $r_0 = 15$ m, $\theta_0 = 0$ rad, $\phi_0 = 0$ rad, $V_{\theta 0} = -0.5$ rad/s, $V_{\phi 0} = 0.2$ rad/s, $V_{r0} = -15$ m/s. From (18), it is seen that this corresponds to $y(0) < 0$ and thus represents a situation that the velocity vector of A lies inside the collision cone. Figure 5 shows the state trajectories. The open loop trajectories are shown with dashed curves. It is seen that $y(t)$ remains constant for all time, indicating that the velocity vector of A lies inside the collision cone for all time. At $t = 0.99$ s, we have $r_m = 0.53 < R$, indicating the occurrence of a collision.

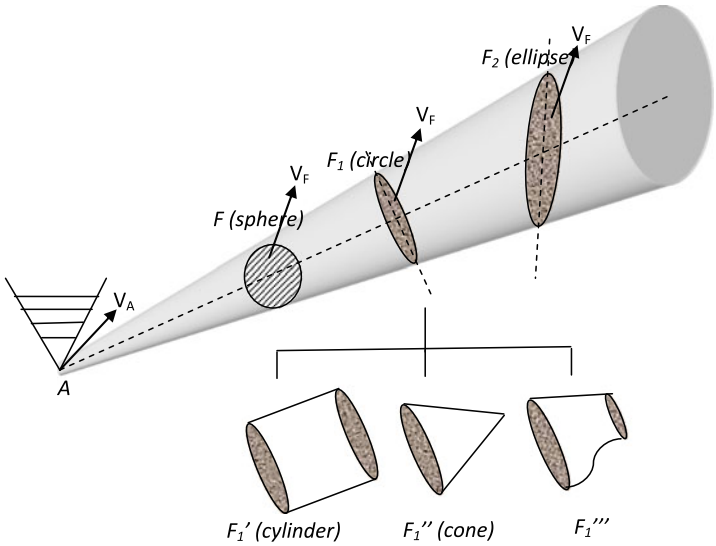

Fig. 6 Examples of a few exact collision cone equivalent objects with a sphere

The same initial condition is then simulated in a closed loop using the acceleration law (23). The closed loop trajectories are shown in Fig. 5 with solid lines. These trajectories are for specific (constant) values of $\gamma = \pi/4$ and $\delta = \pi/3$. Using this guidance law (with $K = 7$ and $\epsilon = 0.1$), collision is avoided as is apparent from the fact that $r_m > R$ and $y(t)$ exponentially goes to zero.

3.3 Collision cone equivalence of a point-sphere system

We demonstrate that collision conditions between a point and a sphere can also directly lead to necessary and sufficient conditions for collision between a point and an additional class of objects. To define this additional class of objects, we use the notion of "exact collision cone equivalence".

Definition 1 An object $\mathcal{P}$ is said to have exact collision cone equivalence with a point-sphere system $(A, \mathcal{F})$ if and only if every ray that originates from A and passes through a point $p \in \mathcal{P}$ also passes through a point $q \in \mathcal{F}$; and vice versa.

Examples of objects with this property are shown in Fig. 6, where $\mathcal{F}$ represents the sphere and $\tilde{\mathcal{F}} = \{\mathcal{F}_1, \mathcal{F}_2, \ldots\}$ are some elements of the set of exact collision cone equivalent objects of the point-sphere system $(A, \mathcal{F})$. Objects that belong to $\tilde{\mathcal{F}}$ include the circular and elliptical planar objects that are conic sections of the cone $\mathcal{E}$, where $\mathcal{E}$ is the circular cone tangential to $\mathcal{F}$ and with vertex at A. The solid objects $\mathcal{F}_1', \mathcal{F}_1'', \mathcal{F}_1'''$ (each of which have a cross section identical to $\mathcal{F}_1$) also have exact collision cone equivalence with $(A, \mathcal{F})$. Also note that $\mathcal{F}_1'''$ is actually a non-convex solid, yet it has exact collision cone equivalence with the convex $\mathcal{F}$ with respect to A.

Now from Lemma 3, we know that if A is on a collision course with $\mathcal{F}$, then there exists a ray AC passing through $\mathcal{F}$, that has the properties $(V_\theta)_{AC} = 0$; $(V_\phi)_{AC} = 0$; $(V_r)_{AC} < 0$. From the definition of $\mathcal{F}_i$, we can see that any such ray will also pass through $\mathcal{F}_i$, and therefore A will also be on a collision course with $\mathcal{F}_i$. Therefore, A is on a collision course with any $\mathcal{F}_i \in \tilde{\mathcal{F}}$ if and only if A is on a collision course with $\mathcal{F}$. Thus the collision cone between A and $\mathcal{F}$ is exactly identical to the collision cone between A and any object belonging to the set $\tilde{\mathcal{F}}$. To get the exact collision condition between A and any object belonging to $\tilde{\mathcal{F}}$, we define an angle ψ such that $\sin(\psi/2) = R/r$ and rewrite (17) as

$$(V_{\theta 0}^2 + V_{\phi 0}^2) \leq (V_{\theta 0}^2 + V_{\phi 0}^2 + V_{r0}^2)\sin^2(\psi/2)$$
$$V_{r0} < 0 \tag{24}$$

It then automatically follows that we can define an avoidance law for any object belonging to $\tilde{\mathcal{F}}$, simply by introducing the angle $\sin(\psi/2) = (R/r)$ in (23). By doing so, the following equation results:

$$\begin{aligned} a_A = {} & (-0.5K(V_\theta^2 + V_\phi^2 + V_r^2))[(V_\theta^2 + V_\phi^2) \\ & - \sin^2(\psi/2)(V_\theta^2 + V_\phi^2 + V_r^2)]/[-V_\theta V_r^2 \cos\gamma \\ & \times \sin(\delta - \theta) + V_\phi V_r^2\{\cos\gamma \sin\phi \cos(\delta - \theta) \\ & - \sin\gamma \cos\phi\} + V_r(V_\theta^2 + V_\phi^2)\{\cos\gamma \cos\phi \cos(\delta - \theta) \\ & + \sin\gamma \sin\phi\}] \end{aligned} \tag{25}$$

We can then state the following:

Theorem 2 *Let the point object A and any $\mathcal{F}_i \in \tilde{\mathcal{F}}$ move such that at $t = t_0$, the velocity vector of A lies inside the collision cone. Then if A uses the acceleration law given in* (25), *(with a sufficiently large $K > 0$), its velocity vector will come out of the collision cone at some time $t_1 \in [t_0, t_m]$.*

Proof Follows from the above discussion. □

3.4 Varying velocities

While the conditions discussed above are exact collision conditions when the objects move with constant velocities, they can also be used for objects with varying (and *a priori* unknown) velocities, by taking the obstacle velocity to be piecewise-constant in time between two successive sensor measurements. In such a scenario, with the sensor measurements being obtained in discrete time k, we can determine the collision cone during the interval $[k, k+1)$ by rewriting (24) as,

$$(V_{\theta k}^2 + V_{\phi k}^2) \leq (V_{\theta k}^2 + V_{\phi k}^2 + V_{rk}^2)\sin^2(\psi_k/2)$$
$$V_{rk} < 0 \tag{26}$$

where, $V_{\theta k}, V_{\phi k}, V_{rk}, \psi_k$ correspond to the measurements obtained at discrete time k.

In the case of varying velocities, (26) represents an approximation to the true (unknown) collision cone. However, even with varying velocities, at the time of collision we have $r_m \leq R$, and therefore a necessary condition for collision is that (26) is satisfied at the time of collision. A sufficient condition for avoidance would then be that (25) be used with sufficiently large K to ensure $y_k > 0 \; \forall \, k$, with y_k being defined accordingly as a discrete-time version of (18).

The associated time to collision $t_{m,k}$ would then be obtained from (16) as,

$$t_{m,k} = \frac{-r_k V_{rk}}{(V_{\theta k}^2 + V_{\phi k}^2 + V_{rk}^2)} \tag{27}$$

Let (β_k, α_k) represent the heading of A at the start of the $k\ th$ time interval and let X_k be the collision cone at that time. Let the boundary of X_k be represented by δX_k, which is defined from (26) as

$$\delta X_k = \{(\beta, \alpha) : (V_{\theta k}^2 + V_{\phi k}^2)$$
$$= (V_{\theta k}^2 + V_{\phi k}^2 + V_{rk}^2)\sin^2(\psi_k/2), V_{rk} < 0\} \tag{28}$$

Now, if (β_k, α_k) is outside X_k, then as long as A and B move with constant velocities, (β_k, α_k) will continue to remain outside X_k, and this will correspond to y_k being positive. On the other hand, if B has a varying velocity, then X_k may evolve with time in a manner so as to contain (β_k, α_k) at some future time, and this will correspond to y_k becoming negative. Note that at each sample, y_k is the square of the anticipated miss distance between the point and the sphere at the time of closest approach. We can then find the (sample-averaged) rate of change of this anticipated miss distance using $\frac{\Delta y}{\Delta T}|_k = \frac{y_k - y_{k-1}}{\Delta T}$ where ΔT represents the sampling time between measurements. A negative value of $\frac{\Delta y}{\Delta T}|_k$ indicates that y_k is decreasing, and so (β_k, α_k) is entering X_k. In this case, we can define a time $t_{go,k}$ which represents an estimate of the time-to-go when (β_k, α_k) will enter the collision cone.

$$t_{go,k} = \frac{y_k}{-\Delta y/\Delta T|_k} \tag{29}$$

After (β_k, α_k) has entered the collision cone, A will collide with B in an additional time interval $t_{m,k}$ defined by (27). Thus at time k, the total time to collision is given by $t_{go,k} + t_{m,k}$. If $\frac{\Delta y}{\Delta T}|_k < 0$ then, based on the value of $t_{go,k}$, an avoidance strategy can be formulated that ensures $\frac{\Delta y}{\Delta T}|_k$ is made non-negative within the time interval $t_{go,k}$—such a strategy would guarantee safety when B is moving with varying velocity. This can be implemented using the dynamic inversion law of (22), using a positive value of the reference signal $w(t)$. This would lead to $\dot{y} = Ke = K(w - y)$ and if $K > 0$ is large enough to ensure that the first order error dynamics decay before time $t_{go,k}$ defined in (29), then it can be guaranteed that (β_k, α_k) will never enter the collision cone, and A will miss the surface of B by a distance of $O(w)$.

4 Point-spheroid collision avoidance

A spheroid is an ellipsoid that has two of its three axes of equal lengths. The equation of a spheroid, centered at the origin and having its three axes along the three co-ordinate axes, is obtained from the quadric surface (1) by substituting $A = 1/a^2$, $B = C = 1/b^2$, $D = E = F = G = H = K = 0$, and $L = -1$ to obtain,

$$x^2/a^2 + y^2/b^2 + z^2/b^2 = 1 \tag{30}$$

Thus, cross-sections taken parallel to two of the three mutually perpendicular co-ordinate planes are ellipses, while cross-sections taken parallel to the third co-ordinate plane are circles. The spheroid is called oblate if $a < b$ and prolate if $a > b$. When $a = b$, the spheroid becomes a sphere. We note that the problem of collision detection between ellipsoids has been discussed in Ju et al. (2001) and Choi et al. (2006, 2009) where trajectories of both the objects are known.

4.1 Exact conditions for collision

Let A be a point object and $\mathcal{F}$ be a spheroid, as represented in Fig. 7. Let C_1 and C_2 represent the two foci of this spheroid. We consider two LOS's, i.e. AC_1 and AC_2. Let r_1 and r_2 represent the distances AC_1 and AC_2, respectively and V_{r1} and V_{r2} represent the components of the relative velocity along AC_1 and AC_2, respectively. Also, $\theta_1, \phi_1, \theta_2, \phi_2$ represent the angular orientations of the lines AC_1 and AC_2 (with their usual meaning with θ representing the azimuth angle and ϕ representing the elevation angle). Then $V_{\theta 1}, V_{\phi 1}, V_{\theta 2}, V_{\phi 2}$ are accordingly defined. In a manner similar to obtaining (9) (corresponding to two points), we now have the following equations:

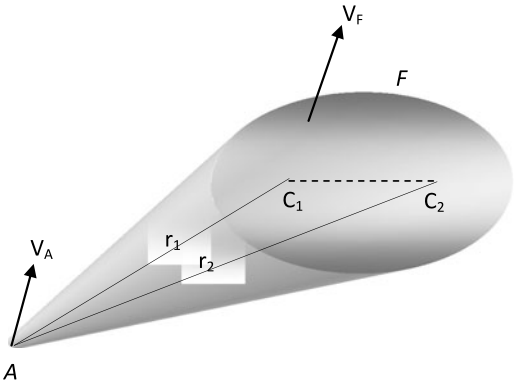

Fig. 7 Collision geometry between a point and a spheroid

$$\begin{aligned}\dot{V}_{\theta i} &= -\dot{\theta}_i(V_{ri}\cos\phi_i - V_{\phi i}\sin\phi_i)\\ \dot{V}_{\phi i} &= -\dot{\phi}_i V_{ri} - \dot{\theta}_i V_{\theta i}\sin\phi_i\\ \dot{V}_{ri} &= \dot{\phi}_i V_{\phi i} + \dot{\theta}_i V_{\theta i}\cos\phi_i;\quad i=1,2\end{aligned} \tag{31}$$

Eliminating $\dot{\theta}_i$ and $\dot{\phi}_i$ from (31), we get

$$\dot{V}_{\theta i}V_{\theta i} + \dot{V}_{\phi i}V_{\phi i} + \dot{V}_{ri}V_{ri} = 0;\quad i=1,2 \tag{32}$$

which on integration yield,

$$\begin{aligned}&{V_{\theta i}}^2 + V_{\phi i}^2 + V_{ri}^2 = V_{\theta 0i}^2 + V_{\phi 0i}^2 + V_{r0i}^2\\ &\quad i=1,2\end{aligned} \tag{33}$$

Equation (33) shows that the relative velocity trajectories of each AC_i lies on a sphere in the (V_θ, V_ϕ, V_r)-space.

The boundary of a spheroid is characterized by the locus of points such that the sum of their distances from the two foci are constant. (Note that this condition holds only for a spheroid—but not for a general ellipsoid). Let us look for the condition when $r_1 + r_2$ is minimum, that is $r_1 + r_2 = (r_1 + r_2)_m$. This will happen if a time t_m exists such that $V_{r1}(t_m) + V_{r2}(t_m) = 0$, which can occur in two ways:

(1) $V_{r1}(t_m) = V_{r2}(t_m) = 0$;
(2) $V_{r1}(t_m) = -V_{r2}(t_m)$.

Point A collides with the spheroid if and only if $(r_1 + r_2)_m \le 2a$ (where $2a$ represents the length of that axis along which the two foci of the spheroid lie—the other two axes have equal lengths). $r_1 = r_{m1}$ when $V_{r1} = 0$, while $r = r_{m2}$ when $V_{r2} = 0$. The occurrence of $(r_1 + r_2)_m$ coincides with the occurrence of $V_{r1} + V_{r2} = 0$. Then one can see that in case (1), $(r_1 + r_2)_m = r_{m1} + r_{m2}$, with the minima to both r_1 and r_2 being attained at the same time instant t_m. We know from (15) that r_{m1} and r_{m2} are obtained as:

$$r_{mi}^2 = r_{0i}^2\left(\frac{V_{\theta 0i}^2 + V_{\phi 0i}^2}{V_{\theta 0i}^2 + V_{\phi 0i}^2 + V_{r0i}^2}\right);\quad i=1,2 \tag{34}$$

Substituting the above in the condition $r_{m1} + r_{m2} \le 2a$, and then simplifying, we get:

$$\begin{aligned}&\left[r_{01}\sqrt{\frac{V_{\theta 01}^2 + V_{\phi 01}^2}{V_{\theta 01}^2 + V_{\phi 01}^2 + V_{r01}^2}}\right.\\ &\left. + r_{02}\sqrt{\frac{V_{\theta 02}^2 + V_{\phi 02}^2}{V_{\theta 02}^2 + V_{\phi 02}^2 + V_{r02}^2}}\right]^2 \le 4a^2\end{aligned} \tag{35}$$

The above inequality thus predicts collision between a point and a spheroid when collision occurs such that the shortest distances between A and each of the foci of the spheroid are attained at the same instant. For the types of collision in case (2), the times of shortest distance of A to the two foci are different and therefore $(r_1 + r_2)_m \ne r_{m1} + r_{m2}$. Let t_{m1} represent the time at which A is closest to point C_1 (i.e., $AC_1(t_{m1}) = r_{m1}$) and t_{m2} represent the time at which A is closest to point C_2 (i.e., $AC_2(t_{m2}) = r_{m2}$). We then have:

$$t_{mi} = -r_{0i}V_{r0i}/(V_{\theta 0i}^2 + V_{\phi 0i}^2 + V_{r0i}^2);\quad i=1,2 \tag{36}$$

Let t_m represent the time at which the sum of the distances from point A to the two foci are the shortest and r_m represent the corresponding sum of the distances at that time t_m. From the above analysis, we can see that if we assume (without loss of generality) that $t_{m1} < t_{m2}$, then $t_{m1} \le t_m \le t_{m2}$. To determine expressions for t_m and r_m, we proceed as follows. We have

$$V_{\theta 1}^2 + V_{\phi 1}^2 + V_{r1}^2 = V_{\theta 01}^2 + V_{\phi 01}^2 + V_{r01}^2 \tag{37}$$

Since $V_{\theta 1}^2 + V_{\phi 1}^2 = r_1\dot{V}_{r1}$ (refer (12)), the above can be written as

$$V_{r1}^2 + r_1\dot{V}_{r1} = V_{\theta 01}^2 + V_{\phi 01}^2 + V_{r01}^2 \tag{38}$$

Substituting $V_{r1}^2 = \dot{r}_1 V_{r1}$, this becomes

$$\dot{r}_1 V_{r1} + r_1\dot{V}_{r1} = V_{\theta 01}^2 + V_{\phi 01}^2 + V_{r01}^2 \tag{39}$$

Integrating (39) and applying the limits from time t_{m1} to t (where t is some time between t_{m1} and t_{m2}),

$$\begin{aligned}\int d(r_1V_{r1}) &= \int_{t_{m1}}^{t}(V_{\theta 01}^2 + V_{\phi 01}^2 + V_{r01}^2)dt\\ \Rightarrow\quad r_1V_{r1} - r_{m1}V_{rm1} &= (V_{\theta 01}^2 + V_{\phi 01}^2 + V_{r01}^2)(t - t_{m1})\end{aligned} \tag{40}$$

Since $V_{rm1} = 0$, the above becomes

$$r_1V_{r1} = (V_{\theta 01}^2 + V_{\phi 01}^2 + V_{r01}^2)(t - t_{m1}) \tag{41}$$

which can be written (after substituting V_{r1} on the left hand side by $\dot{r}_1$) as

$$r_1\dot{r}_1 = (V_{\theta 01}^2 + V_{\phi 01}^2 + V_{r01}^2)(t - t_{m1}) \tag{42}$$

We can again integrate the above from time t_{m1} to t (where again $t_{m1} \le t \le t_{m2}$) to get

$$\begin{aligned}\int_{r_{m1}}^{r_1} r_1dr_1 &= \int_{t_{m1}}^{t}(V_{\theta 01}^2 + V_{\phi 01}^2 + V_{r01}^2)(t - t_{m1})dt\\ \Rightarrow\quad r_1^2 &= r_{m1}^2 + (V_{\theta 01}^2 + V_{\phi 01}^2 + V_{r01}^2)(t - t_{m1})^2\end{aligned} \tag{43}$$

Repeating the above procedure for the ray AC_2, it can be shown that:

$$r_2{}^2 = r_{m2}^2 + (V_{\theta 02}^2 + V_{\phi 02}^2 + V_{r02}^2)(t_{m2} - t)^2 \tag{44}$$

From (43) and (44), we obtain

$$r_1 + r_2 = \sqrt{r_{m1}^2 + (V_{\theta 01}^2 + V_{\phi 01}^2 + V_{r01}^2)(t - t_{m1})^2} + \sqrt{r_{m2}{}^2 + (V_{\theta 02}^2 + V_{\phi 02}^2 + V_{r02}^2)(t_{m2} - t)^2} \tag{45}$$

Differentiating (45) with respect to t, the value of $t = t_m$ at which $r_1 + r_2$ attains a minimum is,

$$t_m = \frac{(r_{m1} t_{m2} + r_{m2} t_{m1})}{(r_{m1} + r_{m2})} \tag{46}$$

Then, r_m can be found by evaluating (45) at $t = t_m$, with t_m given by (46). Now, in the interpretation of (36), use of negative values of t_{m1} and t_{m2} are permissible. This caters to the fact that collision between the point and the spheroid can occur even if either one (but not both) of V_{r01} or V_{r02} is positive. The condition $r_m \le 2a$ can then be written (after some simplification) as:

$$A_1^2(1 + \tau V_1^2) + A_2^2(1 + \tau V_2^2) + 2A_1 A_2 \sqrt{1 + \tau(V_1^2 + V_2^2) + \tau^2 V_1^2 V_2^2} \le 4a^2 \tag{47}$$

where

$$U_i = \sqrt{V_{\theta 0i}^2 + V_{\phi 0i}^2}; \qquad V_i = \sqrt{V_{\theta 0i}^2 + V_{\phi 0i}^2 + V_{r0i}^2}; \qquad A_i = r_{0i} U_i / V_i; \quad i = 1, 2 \tag{48}$$

$$\tau = ((r_{01} V_{r01} / V_1^2 - r_{02} V_{r02} / V_2^2)/(r_{01} U_1 / V_1 + r_{02} U_2 / V_2))^2 \tag{49}$$

Note however that (47) can be a valid collision condition only for non-negative values of t_m. Imposing the condition $t_m \ge 0$ in (46) (after substituting t_{m1} and t_{m2}), we get:

$$V_{r02} \sqrt{V_{\theta 01}^2 + V_{\phi 01}^2} + V_{r01} \sqrt{V_{\theta 02}^2 + V_{\phi 02}^2} \le 0 \tag{50}$$

Note that (35) becomes a special case of (47) (with the former occurring when $t_{m1} = t_{m2}$). Also, as mentioned earlier, (35) is a valid representation for a collision condition only when both $V_{r01} \le 0$ and $V_{r02} \le 0$ are satisfied. And when these are true, (50) is automatically satisfied.

Thus, if a point and a spheroid move with constant velocities and initial conditions that satisfy (47) and (50), then they are headed for a collision. These conditions are both necessary and sufficient.

Note that when the two foci of the spheroid coincide (i.e., $V_{\theta 01} = V_{\theta 02}$, $V_{\phi 01} = V_{\phi 02}$, $V_{r01} = V_{r02}$, $r_{01} = r_{02}$) and the spheroid becomes a sphere, then (47)–(50) do indeed collapse into the conditions for collision between a point and a sphere given in (17). We then have the following lemma:

Lemma 5 *If a point and a spheroid of semi-major axis a are moving with constant velocities such that their initial conditions satisfy* (47)*, then they will continue to satisfy* (47) *for all future time.*

Proof Define a function $y(t)$ as,

$$y(t) = A_1^2(1 + \tau V_1^2) + A_2^2(1 + \tau V_2^2) + 2A_1 A_2 \sqrt{1 + \tau(V_1^2 + V_2^2) + \tau^2 V_1^2 V_2^2} - 4a^2 \tag{51}$$

Differentiating (51) with respect to t, and making appropriate substitutions we get $dy(t)/dt = 0$, which implies that $y(t)$ is constant. Thus, if $y(t) < 0$ initially, it remains so for all future time. □

Lemma 5 is thus a generalization of Lemma 1.

4.2 Collision avoidance

We can use (51) to determine an analytical expression for a guidance law for collision avoidance with the spheroid, using a nonlinear dynamic inversion technique, as shown in Fig. 4, with the state equation $\dot{x} = f(x) + g(x)u$ taking the form:

$$\begin{bmatrix} \dot{r}_1 \\ \dot{\theta}_1 \\ \dot{\phi}_1 \\ \dot{V}_{\theta 1} \\ \dot{V}_{\phi 1} \\ \dot{V}_{r1} \\ \dot{r}_2 \\ \dot{\theta}_2 \\ \dot{\phi}_2 \\ \dot{V}_{\theta 2} \\ \dot{V}_{\phi 2} \\ \dot{V}_{r2} \end{bmatrix} = \begin{bmatrix} V_{r1} \\ V_{\theta 1}/(r_1 \cos\phi_1) \\ V_{\phi 1}/r_1 \\ (-V_{\theta 1} V_{r1} + V_{\theta 1} V_{\phi 1} \tan\phi_1)/r_1 \\ (-V_{\phi 1} V_{r1} - V_{\theta 1}^2 \tan\phi_1)/r_1 \\ (V_{\phi 1}^2 + V_{\theta 1}^2)/r \\ V_{r2} \\ V_{\theta 2}/(r_2 \cos\phi_2) \\ V_{\phi 2}/r_2 \\ (-V_{\theta 2} V_{r2} + V_{\theta 2} V_{\phi 2} \tan\phi_2)/r_2 \\ (-V_{\phi 2} V_{r2} - V_{\theta 2}^2 \tan\phi_2)/r_2 \\ (V_{\phi 2}^2 + V_{\theta 2}^2)/r \end{bmatrix} + \begin{bmatrix} 0 \\ 0 \\ 0 \\ -\cos\gamma \sin(\delta - \theta_1) \\ \cos\gamma \sin\phi_1 \cos(\delta - \theta_1) - \sin\gamma \cos\phi_1 \\ -\cos\gamma \cos\phi_1 \cos(\delta - \theta_1) - \sin\gamma \sin\phi_1 \\ 0 \\ 0 \\ 0 \\ -\cos\gamma \sin(\delta - \theta_2) \\ \cos\gamma \sin\phi_2 \cos(\delta - \theta_2) - \sin\gamma \cos\phi_2 \\ -\cos\gamma \cos\phi_2 \cos(\delta - \theta_2) - \sin\gamma \sin\phi_2 \end{bmatrix} \times a_A \tag{52}$$

In (52), a_A is the acceleration of A, and is applied at an azimuth angle of δ and an elevation angle of γ. The above system of equations is affine in the input a_A. Note that γ and

δ are defined a priori and may be taken to be time-varying or constant. The output equation $y = h(x)$ has the form of (51). Now, we have $\dot{y} = \frac{\partial y}{\partial x}\dot{x}$ and thus

$$\dot{y} = \left[\begin{array}{cccccc} \frac{\partial y}{\partial r_1} & \frac{\partial y}{\partial \theta_1} & \frac{\partial y}{\partial \phi_1} & \frac{\partial y}{\partial V_{\theta 1}} & \frac{\partial y}{\partial V_{\phi 1}} & \frac{\partial y}{\partial V_{r1}} \\ \frac{\partial y}{\partial r_2} & \frac{\partial y}{\partial \theta_2} & \frac{\partial y}{\partial \phi_2} & \frac{\partial y}{\partial V_{\theta 2}} & \frac{\partial y}{\partial V_{\phi 2}} & \frac{\partial y}{\partial V_{r2}} \end{array}\right] \times \left[\dot{r}_1\ \dot{\theta}_1\ \dot{\phi}_1\ \dot{V}_{\theta 1}\ \dot{V}_{\phi 1}\ \dot{V}_{r1}\ \dot{r}_2\ \dot{\theta}_2\ \dot{\phi}_2\ \dot{V}_{\theta 2}\ \dot{V}_{\phi 2}\ \dot{V}_{r2}\right]^T \quad (53)$$

Define an error signal $e(t) = w(t) - y(t)$, where $w(t)$ is the reference input indicated in Fig. 4. Thus $\dot{y} = \dot{w} - \dot{e}$. Taking $w(t) = 0\ \forall t$ and enforcing the error dynamics to be $\dot{e} = -Ke$, (with $K > 0$), we get $\dot{y} = Ke = -Ky$. Substitute this in (53) to eventually obtain:

$$\begin{aligned} a_A = -Ky/\Bigg[& -\cos\gamma\left(\frac{\partial y}{\partial V_{\theta 1}}\sin(\delta-\theta_1) + \frac{\partial y}{\partial V_{\theta 2}}\sin(\delta-\theta_2)\right) \\ & + \frac{\partial y}{\partial V_{\phi 1}}(\cos\gamma\sin\phi_1\cos(\delta-\theta_1) - \sin\gamma\cos\phi_1) \\ & + \frac{\partial y}{\partial V_{\phi_2}}(\cos\gamma\sin\phi_2\cos(\delta-\theta_2) - \sin\gamma\cos\phi_2) \\ & - \frac{\partial y}{\partial V_{r1}}(\cos\gamma\cos\phi_1\cos(\delta-\theta_1) + \sin\gamma\sin\phi_1) \\ & - \frac{\partial y}{\partial V_{r2}}(\cos\gamma\cos\phi_2\cos(\delta-\theta_2) + \sin\gamma\sin\phi_2)\Bigg] \end{aligned} \quad (54)$$

Equation (54) is a guidance law that will drive $y(t)$ to zero. In this equation, the partial derivatives of y can be easily computed analytically. Note that any $K > 0$ will guarantee that $y(t)$ exponentially decays to zero (since the error dynamics $e(t)$ are essentially first order). Further, when $y(t)$ becomes zero it corresponds to the physical scenario of the velocity vector of A being aligned with the boundary of the collision cone. We however need to choose K to be at least as large as to ensure that $y(t)$ decays to zero before the time t_m defined in (46). Now in theory, the exponential nature of $y(t)$ will mean that $y(t)$ goes to zero only as $t \to \infty$. However, if the original semi-major axis of the spheroid a is increased to $a + \epsilon$, where $\epsilon > 0$ is a small number, it can be ensured that $y(t)$ corresponding to a will go to zero in finite time. These results lead to the following theorem.

Theorem 3 *If a point and a spheroid are moving such that at $t = t_0$, the velocity vector of the point lies inside the collision cone (defined by (47) and (50)), then if the point uses the acceleration law given in (54), its velocity vector will come out of the collision cone at some time $t_1 \in [t_0, t_m]$. If the spheroid moves with constant velocity for all $t \geq t_0$ and the point moves with constant velocity for all $t \geq t_1$, collision avoidance is guaranteed.*

Proof Follows from the analysis given above. □

Example 2 Consider a point and a spheroid of semi-major axis $a = 50$ m, with initial conditions $r_{01} = 122.26$ m, $\theta_{01} = 0.20$ rad, $\phi_{01} = -0.23$ rad, $V_{\theta 01} = 1.51$ rad/s, $V_{\phi 01} = -0.91$ rad/s, $V_{r01} = -7.18$ m/s, $r_{02} = 83.75$ m, $\theta_{02} = -0.13$ rad, $\phi_{02} = 0.16$ rad, $V_{\theta 02} = -0.94$ rad/s, $V_{\phi 02} = 1.99$ rad/s, $V_{r02} = -7.06$ m/s. From (51), it is seen that $y(0) < 0$ and this represents a situation that the velocity vector of A lies inside the collision cone. Figure 8 shows the state trajectories. The open loop trajectories are shown as dashed curves. It is seen that $y(t)$ remains negative for all time, indicating that the velocity vector of A lies inside the collision cone for all time. At around $t = 12$ s, we have $r_m = 60 < 2a$, indicating the occurrence of collision.

The same initial condition is then simulated in a closed loop using the acceleration law in (54). The closed loop trajectories are shown in Fig. 8 with solid lines. These closed loop trajectories are for specific (constant) values of γ and δ. Using this guidance law (with $K = 2$ and $\epsilon = 0.1$), collision is avoided as is apparent from the fact that $r_m = 100 + \epsilon$ and $y(t)$ exponentially goes to zero (Fig. 9).

4.3 Collision cone equivalence of a point-spheroid system

We show that the conditions for collision between a point and a spheroid also directly lead to conditions for collision between a point and an additional class of objects.

Definition 2 An object $\mathcal{P}$ is said to have exact collision cone equivalence with a point-spheroid system $(A, \mathcal{F})$ if and only if every ray that originates from A and passes through a point $p \in \mathcal{P}$ also passes through a point $q \in \mathcal{F}$; and vice versa.

Let $\tilde{\mathcal{F}}$ represent the set of objects that have collision cone equivalence with $(A, \mathcal{F})$. Some examples of objects in $\tilde{\mathcal{F}}$ include an ellipse, an ellipsoid and a circle oriented such that the normal to its plane does not pass through the point A. By using the above definition, and proceeding along the same lines as in the case of point-sphere collision equivalence, we can see that A is on a collision course with any $\mathcal{F}_i \in \tilde{\mathcal{F}}$ if and only if A is on a collision course with the spheroid $\mathcal{F}$. Then (47)–(50) can be used to determine the exact collision cone between A and any object $\mathcal{F}_i \in \tilde{\mathcal{F}}$. Since the collision cone for the spheroid F is identical with that of any $\mathcal{F}_i$, it automatically follows that the avoidance maneuver (54) used for $\mathcal{F}$ will also be a valid avoidance maneuver for any $\mathcal{F}_i$.

Theorem 4 *Let the point object A and any $\mathcal{F}_i \in \tilde{\mathcal{F}}$ move such that at $t = t_0$, the velocity vector of A lies inside the collision cone. Then, if A uses the acceleration law given in (54) (with a sufficiently large $K > 0$), its velocity vector will come out of the collision cone at some time $t_1 \in [t_0, t_m]$.*

Proof Follows from the above discussion. □

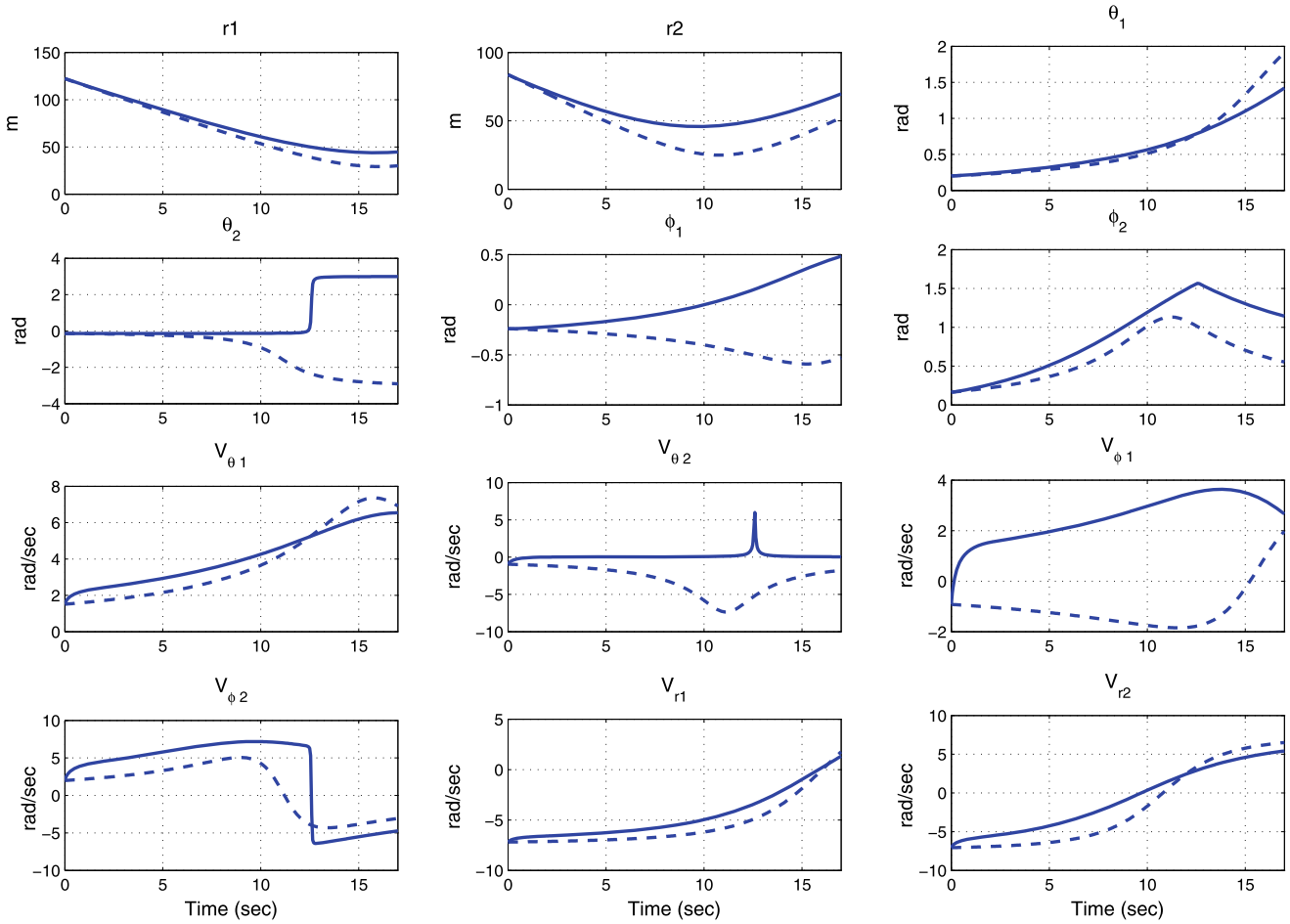

Fig. 8 State trajectories in open loop (- - -) and closed loop (—) for a point-spheroid engagement

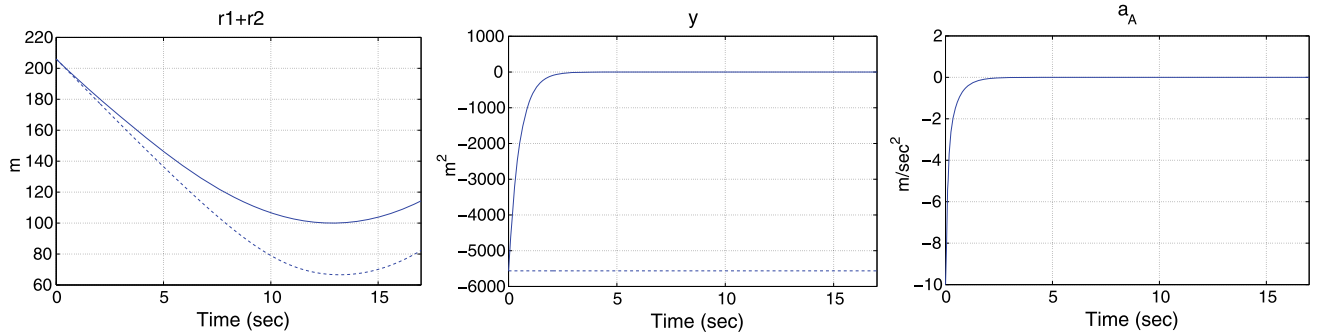

Fig. 9 Input and output trajectories in open loop (- - -) and closed loop (—) for a point-spheroid engagement

4.4 Varying velocities

When the objects move with varying velocities and the sensor measurements are obtained in discrete time k, we can determine the collision cone during the interval $[k, k+1)$ by continuing to use (47) after rewriting (49) and (50) with '0' in the subscript replaced by 'k'.

$$U_i = \sqrt{V_{\theta i,k}^2 + V_{\phi i,k}^2}$$

$$V_i = \sqrt{V_{\theta i,k}^2 + V_{\phi i,k}^2 + V_{ri,k}^2} \tag{55}$$

$$A_i = r_{i,k} U_i / V_i; \quad i = 1, 2$$

$$\tau = ((r_{1,k} V_{r1,k} / V_1^2 - r_{2,k} V_{r2,k} / V_2^2) / (r_{1,k} U_1 / V_1 + r_{2,k} U_2 / V_2))^2 \tag{56}$$

$$V_{r2k} \sqrt{V_{\theta 1k}^2 + V_{\phi 1k}^2} + V_{r1k} \sqrt{V_{\theta 2k}^2 + V_{\phi 2k}^2} \leq 0 \tag{57}$$

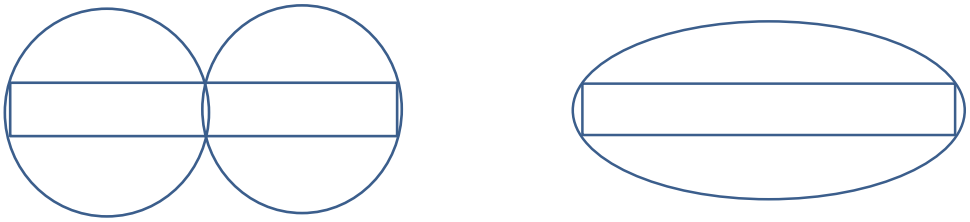

Fig. 10 Approximating a rectangle by (**a**) two circles and (**b**) a single ellipse

where, $V_{\theta 1k}$, $V_{\phi 1k}$, etc., correspond to the measurements obtained at discrete time k. As discussed in the point-sphere section in the varying velocity case, a necessary condition for collision is that (47) and (57) are satisfied at the time of collision. A sufficient condition for avoidance would be that (54) be used with sufficiently large K so as to ensure that $y_k > 0\ \forall k$, where y_k is the discrete time version of (51). We can also compute the time to collision $t_{m,k}$, by adapting (46) in the form

$$t_{m,k} = \frac{(r_{m1,k}t_{m2,k} + r_{m2,k}t_{m1,k})}{(r_{m1,k} + r_{m2,k})} \tag{58}$$

with $r_{m1,k}$ and $r_{m2,k}$ defined as

$$r_{mi,k}{}^2 = r_{i,k}{}^2 \left(\frac{V_{\theta i,k}{}^2 + V_{\phi i,k}{}^2}{V_{\theta i,k}{}^2 + V_{\phi i,k}{}^2 + V_{ri,k}{}^2} \right); \quad i = 1, 2 \tag{59}$$

and with $t_{m1,k}$ and $t_{m2,k}$ defined as

$$t_{mi,k} = -r_{i,k}V_{ri,k}/(V_{\theta i,k}^2 + V_{\phi i,k}^2 + V_{ri,k}^2); \quad i = 1, 2 \tag{60}$$

Let (β_k, α_k) represent the heading of A at the start of the kth time interval and let X_k be the collision cone at the same time. Let the boundary of X_k be represented by δX_k, which is defined as

$$\begin{aligned} \delta X_k = \Big\{ (\beta_k, \alpha_k) : {} & A_1^2(1 + \tau V_1^2) + A_2^2(1 + \tau V_2^2) \\ & + 2A_1A_2\sqrt{1 + \tau(V_1^2 + V_2^2) + \tau^2 V_1^2 V_2^2} \\ & - 4a^2 = 0, \\ & V_{r2k}\sqrt{V_{\theta 1k}^2 + V_{\phi 1k}^2} + V_{r1k}\sqrt{V_{\theta 2k}^2 + V_{\phi 2k}^2} \le 0 \Big\} \end{aligned} \tag{61}$$

Now, if (β_k, α_k) is outside X_k, then as long as A and B move with constant velocities, (β_k, α_k) will continue to remain outside X_k, and this will correspond to y_k being positive. On the other hand, if B moves with varying velocity, then X_k may evolve with time in a manner so as to contain (β_k, α_k) at some future time, and this will correspond to y_k being negative. Note that at each sample, y_k gives the square of the anticipated miss distance between the point and the spheroid at the time of closest approach. Then, we can again find the sample-averaged rate of change of this anticipated miss distance $\frac{\Delta y}{\Delta T}|_k$. If this quantity is negative, it would mean that (β_k, α_k) is entering X_k, in which case we can use (29) to define $t_{go,k}$ as the time-to-go by when (β_k, α_k) will enter the collision cone. By using the dynamic inversion law with a positive value of the reference signal $w(t)$, i.e., taking $\dot{y} = Ke = K(w - y)$ and ensuring that $K > 0$ is large enough to ensure that the first order error dynamics decay before time $t_{go,k}$ defined in (29), it can be guaranteed that (β_k, α_k) will never enter the collision cone.

4.5 Some approximation issues

We now compare the extent of over-approximation achieved when a long slender object is approximated by a single ellipse as opposed to using multiple circles. For the purpose of illustration, we use a rectangle of width w and height h. In the preceding sections, we have demonstrated that to determine the collision cone and avoidance maneuver for an ellipse, we require sensor measurements (range and velocity) associated with only two points, namely the foci of the ellipse. The collision cone and avoidance maneuver for a circle requires sensor measurements associated with only one point, namely the center of the circle. So, if we have a constraint that sensor measurements can be taken from only two points, what is the smallest possible over-approximation achievable by using two circles and how does this compare to the smallest possible over-approximation achievable using a single ellipse?

It can be seen that, by using two circles C_1 and C_2 to completely enclose the rectangle (Fig. 10a), the smallest possible value of the quantity $\Delta A_{circles}$ = Area of C_1 + Area of C_2 – Area of $C_1 \cap C_2 - wh$ is given by

$$\Delta A_{circles} = R^2(2\pi - 2\chi + 0.5\sin 2\chi) - wh \tag{62}$$

where, $R = \sqrt{w^2/16 + h^2/4}$ represents the radii of C_1 and C_2 of smallest area that enclose the rectangle and $\chi = \tan^{-1}(2h/w)$. On the other hand, by using a single ellipse of the smallest area that completely encloses the rectangle (Fig. 10b), we get $\Delta A_{ellipse}$ = Area of ellipse – wh, as

$$\Delta A_{ellipse} = (\pi/2 - 1)wh \tag{63}$$

Let $w = \kappa h$. Figure 11 is a plot of $\Delta A_{circles}$ and $\Delta A_{ellipse}$ versus κ. For $\kappa > 3$, the extent of over-approximation achieved by using two circles is greater than that achieved by using a single ellipse. Furthermore, the value of this over-approximation keeps increasing with increasing κ. In an environment cluttered with many obstacles, it is better to have a smaller over-approximation since this makes more free space available for navigation. The above analysis can also

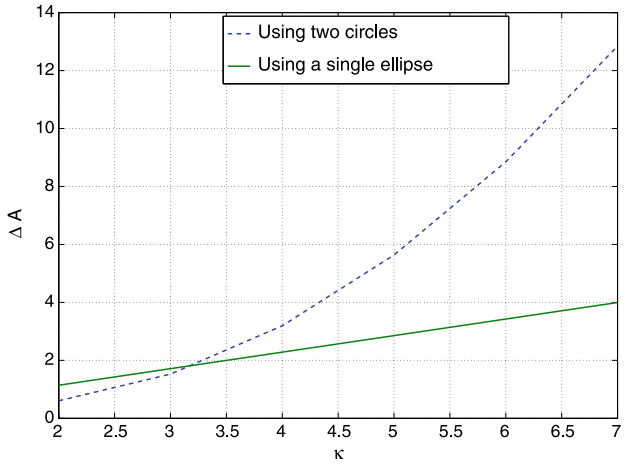

Fig. 11 Comparison of over-approximation of a rectangle by using a single ellipse as opposed to two circles

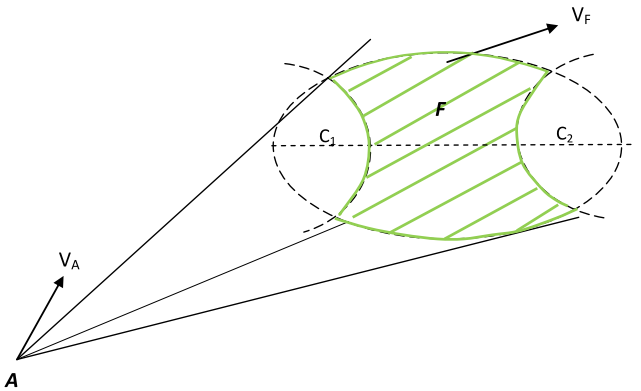

Fig. 12 A nonconvex section obtained as the intersection of a spheroid and a hyperboloid

be used to determine that for $\kappa = 5$, we would require at least 3 circles to achieve the same (or better) level of over-approximation as a single ellipse, while for $\kappa = 6$ we would require at least 4 circles. This thus demonstrates the benefit of using a quadric surface such as a single ellipse in lieu of multiple circles, for bounding elongated objects. A similar analysis can be performed for three-dimensional objects.

5 Point-confocal quadric collision avoidance

We now consider collision avoidance for a class of objects with nonconvex cross-section. An example is given in Fig. 12, which shows the intersection of a spheroid and a hyperboloid of two sheets. The shaded region in this figure (i.e., the intersection of the spheroid and the complement of the two sheeted hyperboloid) is nonconvex. The figure and the discussion below considers confocal quadrics (that is, both quadric surfaces—the spheroid and the hyperboloid have the same foci), but it would be straightforward to generalize this to situations when the quadrics do not share the same set of foci.

Let C_1 and C_2 represent the two foci. The equation of a two-sheeted hyperboloid, obtained by revolving a hyperbola about its focal axis C_1C_2, is obtained from the quadric equation (1) by substituting $A = 1/a_h^2$, $B = C = -1/b_h^2$, $D = E = F = G = H = K = 0$, and $L = -1$ to obtain,

$$x^2/a_h^2 - y^2/b_h^2 - z^2/b_h^2 = 1 \tag{64}$$

If r_1 and r_2 represent the distances of any point on this hyperboloid from C_1 and C_2, respectively, they satisfy the equation $|r_1 - r_2| = 2a_h$. Recall also that if r_1 and r_2 represent the distances of any point on the spheroid from C_1 and C_2, they satisfy the equation $r_1 + r_2 = 2a$. We can then determine the exact collision condition between a point and the object $\mathcal{F}$ as follows.

Let r_1 and r_2 represent the distances of the point A to each of the two foci and let the relative velocity components be defined accordingly. Note that for A to be on a collision course with object $\mathcal{F}$ of Fig. 12, it first needs to collide with the spheroid shown in the figure. Let t_m represent the time at which $r_1 + r_2$ attains its minimum value, as obtained in (46). At this value of t_m, we compute the quantity $|r_1 - r_2|$, which is given as

$$\begin{aligned} &|r_1(t_m) - r_2(t_m)| \\ &\quad = \Big|\sqrt{r_{m1}^2 + (V_{\theta 01}^2 + V_{\phi 01}^2 + V_{r01}^2)(t_m - t_{m1})^2} \\ &\qquad - \sqrt{r_{m2}^2 + (V_{\theta 02}^2 + V_{\phi 02}^2 + V_{r02}^2)(t_{m2} - t_m)^2}\Big| \end{aligned} \tag{65}$$

Imposing the requirement that $(r_1(t_m) - r_2(t_m))^2 \leq 4a_h^2$ then leads to the following condition:

$$\begin{aligned} &A_1^2(1 + \tau V_1^2) + A_2^2(1 + \tau V_2^2) \\ &\quad - 2A_1A_2\sqrt{1 + \tau(V_1^2 + V_2^2) + \tau^2 V_1^2 V_2^2} \leq 4a_h^2 \end{aligned} \tag{66}$$

where, the quantities U_1, U_2, V_1, V_2 and τ are defined as in (49).

Thus, if a point and an object $\mathcal{F}$ move with constant velocities and initial conditions satisfy (47), (50) and (66), then they are headed for a collision. These conditions are both necessary and sufficient for collision.

Lemma 6 *If a point and a confocal quadric $\mathcal{F}$ of semi-major axes a and a_h move with constant velocities and initial conditions that satisfy* (47) *and* (66)*, then they will continue to satisfy* (47) *and* (66) *for all future time.*

Proof By Lemma 5, the above has already been proved by defining $y(t)$ to correspond to (47). In the case of (66), we can similarly define $y_h(t)$ as,

$$\begin{aligned} y_h(t) = {} & A_1^2(1 + \tau V_1^2) + A_2^2(1 + \tau V_2^2) \\ & - 2A_1A_2\sqrt{1 + \tau(V_1^2 + V_2^2) + \tau^2 V_1^2 V_2^2} \\ & - 4a_h^2 \end{aligned} \tag{67}$$

and proceed along lines similar to Lemma 5. □

We can use (67) to derive an acceleration law for avoidance, again using a dynamic inversion technique. The state equation would be identical to (52). Using the output equation as in (67) would lead to an acceleration law given as:

$$
\begin{aligned}
a_A = -K y_h \Big/ \Bigg[& -\cos\gamma \left(\frac{\partial y_h}{\partial V_{\theta 1}} \sin(\delta - \theta_1) \right. \\
& \left. + \frac{\partial y_h}{\partial V_{\theta 2}} \sin(\delta - \theta_2) \right) \\
& + \frac{\partial y_h}{\partial V_{\phi 1}} (\cos\gamma \sin\phi_1 \cos(\delta - \theta_1) - \sin\gamma \cos\phi_1) \\
& + \frac{\partial y_h}{\partial V_{\phi_2}} (\cos\gamma \sin\phi_2 \cos(\delta - \theta_2) - \sin\gamma \cos\phi_2) \\
& - \frac{\partial y_h}{\partial V_{r1}} (\cos\gamma \cos\phi_1 \cos(\delta - \theta_1) + \sin\gamma \sin\phi_1) \\
& - \frac{\partial y_h}{\partial V_{r2}} (\cos\gamma \cos\phi_2 \cos(\delta - \theta_2) + \sin\gamma \sin\phi_2) \Bigg]
\end{aligned}
\tag{68}
$$

Note that (54) would also be a valid acceleration law to avoid $\mathcal{F}$. By using (54), A would avoid $\mathcal{F}$ by passing close to the spheroidal surface, whereas by using (68), A would avoid $\mathcal{F}$ by passing close to the hyperboloid surface. Which of the two acceleration laws to choose in a given situation would depend on the relative locations of other obstacles neighboring $\mathcal{F}$. We however need $K > 0$ to be at least as large as to ensure that $y(t)$ (or $y_h(t)$) decays to zero before the time t_m defined in (46). Again, by increasing the original semi-major axes of $\mathcal{F}$ to $a + \epsilon$ (or $a_h + \epsilon$), where ϵ is a small number, it can be ensured that $y(t)$ ($y_h(t)$) corresponding to a (a_h) will go to zero in finite time. These results lead to the following theorem.

Theorem 5 *If a point and object $\mathcal{F}$ are moving such that at $t = t_0$, the velocity vector of the point lies inside the collision cone, then if the point uses the acceleration law given in (54) or (68), its velocity vector will come out of the collision cone at some time $t_1 \in [t_0, t_m]$. If $\mathcal{F}$ moves with constant velocity for all $t \geq t_0$ and the point moves with constant velocity for all $t \geq t_1$, collision avoidance is guaranteed.*

Proof Follows from the analysis given above. □

The notion of exact collision cone equivalence can be used to get collision conditions for a class of objects with nonconvex cross sections. Additionally, arbitrary nonconvex shapes can be approximated with shapes such as the above. Furthermore, when the objects are moving with varying (and *a priori* unknown) velocities and the sensor measurements are obtained in discrete time k, we again use a piece-wise constant approximation and determine the collision cone during the interval $[k, k+1)$ by rewriting (66) with '0' replaced by 'k' in the subscript. Furthermore, in the time-varying velocity case, $t_{m,k}$ is given by (58)–(60). Finally, we can use (66) in conjunction with (61) to define the boundary of the collision cone δX_k and subsequently obtain the square of the anticipated miss-distance as well as $t_{go,k}$ using (67) and (29), respectively. Similar to the discussion in the previous sections, these quantities can be used to generate a dynamic inversion based avoidance maneuver that will guarantee safety even when $\mathcal{F}$ moves with varying velocity.

6 Collision avoidance between a point and an arbitrary object moving in space

6.1 Planar section of exact collision cone

The focus in the previous sections has been on characterizing and using 3-D collision cones for collision avoidance using quadric surfaces. However, as pointed out earlier, the literature on 2-D collision cones is rather extensive and these results have been used by several researchers to determine collision cones in 3-D for spherical bounding boxes (for example, see Watanabe et al. 2006a, 2006b, 2007a, 2007b; Carbone et al. 2006; Gross et al. 2004). A reason for the extensive applications of 2-D collision cones is the simplicity of the analytical expressions which are easily extended to the spherical bounding box case. But, if one wishes to use the simple 2-D results to obtain collision cones for 3-D arbitrarily shaped objects, without resorting to the conservative spherical bounding box assumption, then one can use the idea of constructing planar sections of the exact 3-D spatial collision cone by considering planes that contain the relative velocity vector, the point A, and passes through the arbitrarily shaped object B. This will then allow us to determine avoidance maneuvers on that plane. We first state the following:

Lemma 7 *Consider an engagement between a point object A and a circular object B of radius R moving with constant velocities such that $\vec{V}_A$, $\vec{V}_B$ and B all lie on the same plane $\mathcal{P}$ in space. Then, A is on a collision course with B if and only if (17) is satisfied with $V_{\theta 0}$, $V_{\phi 0}$ and V_{r0} representing the relative velocity components of the line joining A and the center of the circular object B.*

Proof We can construct an imaginary sphere $\mathcal{F}$ such that B is a great circle of $\mathcal{F}$. Now, if A is on a collision course with B, then A is also on a collision course with $\mathcal{F}$. However, if A is not on a collision course with B, then A is also not on a collision course with $\mathcal{F}$. This is due to the fact that collision between A and $\mathcal{F}$ (if it occurs) can happen only on the plane $\mathcal{P}$. Thus A is on a collision course with B if and only if A is on a collision course with $\mathcal{F}$. The proof then follows from the above discussion. Note that this lemma represents a planar version of Lemma 4. □

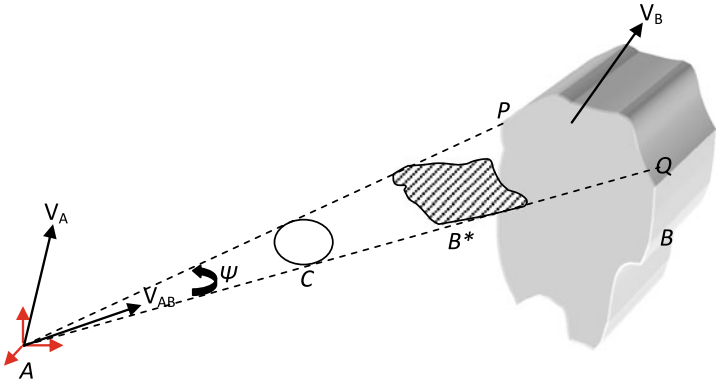

Fig. 13 Collision between a point and an arbitrary object in the case when $\psi < \pi$ and B^* is not disjoint

An important corollary of Lemma 7 is that by using the dynamic inversion based guidance law (25) with a (δ, γ) pair such that $\vec{V}_A$ remains on $\mathcal{P}$, A will avoid collision with B. Since collision between A and $\mathcal{F}$ can occur only on the plane $\mathcal{P}$, therefore collision avoidance between A and $\mathcal{F}$ on the plane $\mathcal{P}$ automatically ensures collision avoidance between A and $\mathcal{F}$ in 3-D space. Note however, that this represents only a sufficient condition for A to avoid $\mathcal{F}$. There can certainly be other maneuvers (in which $\vec{V}_A$ does not remain on the plane $\mathcal{P}$) with which A can avoid $\mathcal{F}$.

Refer to Fig. 13 which shows the collision geometry between a point object A and an arbitrary object B. Construct the plane $\mathcal{P}$ as above, that contains $\vec{V}_A$ and $\vec{V}_B$ originating at A. If $\mathcal{P}$ does not intersect the object B, then it implies that the relative velocity vector (placed at A) does not pass through B and it is guaranteed that A is not on a collision course with B. On the other hand, if $\mathcal{P}$ does intersect the object B, then let B^* represent the intersection of $\mathcal{P}$ with B. The following cases then arise:

(a) If B^* is not disjoint (i.e., B^* is a single object and not a union of several disjoint objects), then let ψ denote the angle of the sector formed by the two lines AP and AQ that are tangential to B^*. We can then construct an imaginary circle C that lies on $\mathcal{P}$ and is tangential to AP and AQ (refer Fig. 13). If $\psi < \pi$, A is on a collision course with B^* if and only if A is on a collision course with C. Using the results of Lemma 6, noting that $\sin\frac{\psi}{2} = \frac{R}{r}$, we can see that A is on a collision course with B if and only if (24) is satisfied, with V_{r0}, $V_{\theta 0}$ and $V_{\phi 0}$ representing the relative velocity components of the angular bisector of the above mentioned sector.

(b) If B^* is disjoint and comprises of n distinct parts $B_1^*, B_2^*, \ldots, B_n^*$ (that is $B^* = B_1^* \cup B_2^* \cup \cdots \cup B_n^*$; this can occur in situations where B is non-convex—see Fig. 14), then let ψ_i denote the angle of the sector formed by the lines originating at A and tangential to the i-th part of B^*. When $\psi_i < \pi, \forall i$ A is on a collision course with B if and only if the following inequality is satisfied for some part i.

$$(V_{\theta 0i}^2 + V_{\phi 0i}^2) \leq (V_{\theta 0i}^2 + V_{\phi 0i}^2 + V_{r0i}^2)\sin^2\frac{\psi_i}{2}$$
$$V_{r0i} < 0 \tag{69}$$

where, $V_{\theta 0i}$, $V_{\phi 0i}$ and V_{r0i}, are the relative velocity components of the angular bisector of the i-th sector.

We point out that in case (a), (24) cannot be used to compute the spatial collision cone between A and B, but can be used to compute a *planar* section of the spatial collision cone. Indeed, by taking the intersection of the plane $\mathcal{P}$ with the spatial cone generated by (24), we get an exact representation of the planar section of the spatial collision cone between A and B, denoted as X_P. Thus, if we define

$$\mathcal{N}_1 = \left\{(\beta, \alpha) : (V_{\theta 0}^2 + V_{\phi 0}^2) \leq (V_{\theta 0}^2 + V_{\phi 0}^2 + V_{r0}^2)\sin^2\frac{\psi}{2}\right\} \tag{70}$$

$$\mathcal{N}_2 = \{(\beta, \alpha) : V_{r0} < 0\}$$

then X_P is defined as

$$X_P = \left\{(\beta, \alpha) : \mathcal{N}_1 \bigcap \mathcal{N}_2 \bigcap \mathcal{P}\right\} \tag{71}$$

This X_P can be used to determine avoidance maneuvers on plane $\mathcal{P}$. For this, we proceed as follows. Consider case (a). Assume the velocity vector of A lies inside X_P. First, we determine the time of closest approach t_m associated with B^*. For all rays originating from A and passing through B^*, identify the point Q on B^* that satisfies $(V_\theta)_{AQ} = 0$; $(V_\phi)_{AQ} = 0$; $(V_r)_{AQ} < 0$. This point Q can be determined through use of a bisection algorithm. (This is possible since V_θ and V_ϕ are both continuous functions of θ and ϕ, they vary continuously as we traverse from ray AP to ray AQ. Furthermore, $V_\theta = V_\phi = 0, V_r < 0$ can occur only for a unique ray.) Then A is on an imminent collision with point Q on B^*. Determine t_m from the expression $t_m = -\frac{(r_0)_{AQ}}{(V_{r0})_{AQ}}$. If A changes its velocity vector so that its heading lies outside X_P, and it does so within a time $t_1 \in (t_0, t_m)$, then it is guaranteed that A will not collide with B^* and consequently, A will also not collide with B.

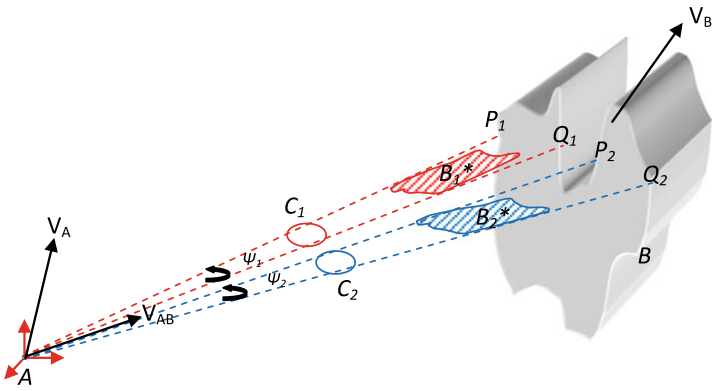

Fig. 14 Collision between a point and an arbitrary object in the case when $\psi < \pi$ and B^* is disjoint

This can be achieved by using the acceleration law given in (25) and applying this law using a (δ, γ) pair that keeps $\vec{V}_A$ on the plane $\mathcal{P}$. A similar set of statements can be made for case (b).

In the variable velocity case (with the velocity of the obstacle unknown *a priori*), we can make use of a piecewise constant velocity assumption and rewrite (71) with 'k' in the subscript, to determine a planar section of the collision cone X_{Pk} at each k.

6.2 Approximation to spatial collision cone

The above scheme is suited for fast computations in that it allows us to construct a single plane in space and compute an avoidance maneuver on that plane. It is however restrictive in that it can be used to generate avoidance maneuvers only on that single plane. This could be inadequate in a dynamic environment cluttered with many moving obstacles, since the avoidance maneuver generated on that plane could lead to collision with a different obstacle. In such scenarios, it might be a better option to obtain an approximation to the full 3-D collision cone, so as to have a larger set of avoidance maneuvers available. To do so, the above scheme can be readily extended by rotating the plane $\mathcal{P}$ about $\vec{V}_B$ to generate n different planes $P_1, P_2, \ldots, P_n$. On each plane, planar sections of the 3-D collision cone can be computed (in the manner discussed above), denoted as $X_1, X_2, \ldots, X_n$. These n collision cones can then be suitably combined (using a combining operation denoted by $\vee$) on the pair of cones X_i and X_{i+1}, for $i = 1, 2, \ldots, n-1$ and then taking the union of the resulting cones. Thus, the three dimensional cone X is given by

$$X = (X_1 \vee X_2) \bigcup (X_2 \vee X_3) \bigcup \cdots \bigcup (X_{n-1} \vee X_n) \quad (72)$$

where the operation $\vee$ is defined as follows:

Case 1. When the cones do not intersect (except at point A): In this case,

$$X_i \vee X_{i+1} = \mathrm{Co}(X_i, X_{i+1}) \quad (73)$$

where, $\mathrm{Co}(A, B)$ denotes the convex hull of the sets A and B. Figure 15 illustrates this case.

Case 2. When the cones intersect: This is the case when the shifted $\vec{V}_B$ lies in both X_i and X_{i+1}. The cones then intersect along the $\vec{V}_B$ line, which divides each cone into two half cones (X_{i_1}, X_{i_2}) and (X_{i+1_1}, X_{i+1_2}). The combined cone is then two three-dimensional cones joined at the $\vec{V}_B$ line, each of which is the convex hull of two half-cones, one from each original cone. The half cones to be used for this operation are determined by the direction along which the plane P_i is rotated to generate P_{i+1}. Thus,

$$X_i \vee X_{i+1} = \mathrm{Co}(X_{i_1}, X_{i+1_1}) \bigcup \mathrm{Co}(X_{i_2}, X_{i+1_2}) \quad (74)$$

The three dimensional cone so obtained would be an approximation of the exact collision cone. Note that the larger the number of planes, the better is the approximation to the exact collision cone. This 3-D cone will then give information of the safe collision-avoidance maneuvers possible in 3-D space. To obtain guaranteed collision avoidance with the sectioning strategy, we proceed as follows: Enclose the arbitrary object by an appropriate quadric surface—say, a bounding ellipse. Then perform the sectioning on the bounding ellipse. If the convex hull of these sections completely encloses the arbitrary object, then the ensuing 3-D collision cone would be an over-approximation to the true collision cone. Now, the larger the size of the bounding ellipse, the smaller the number of sections that would be required to achieve this over-approximation. For a given size of the bounding ellipse, a guideline to obtaining the number of planes n is demonstrated in the following example.

Example 3 Consider an arbitrary object shown in Fig. 16 for which the approximate collision cone needs to be determined. This object is bounded by an ellipse as shown. Three cases corresponding to three different sizes of the bounding ellipse are shown. In Fig. 16(a), we consider a large bounding ellipse and it is seen that in this case, it is sufficient to have just two sectioning planes P_1 and P_2. When we determine the points of intersection of the planes P_1 and P_2 with the bounding ellipse, and then take the convex hull of these points, this convex hull encloses the inner object. Two planes thus represent the smallest number of planes on which to

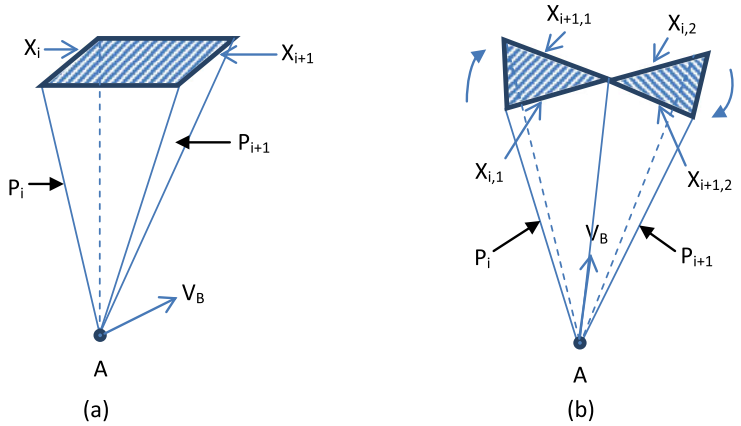

Fig. 15 (**a**) When planar cones do not intersect (**b**) When planar cones intersect

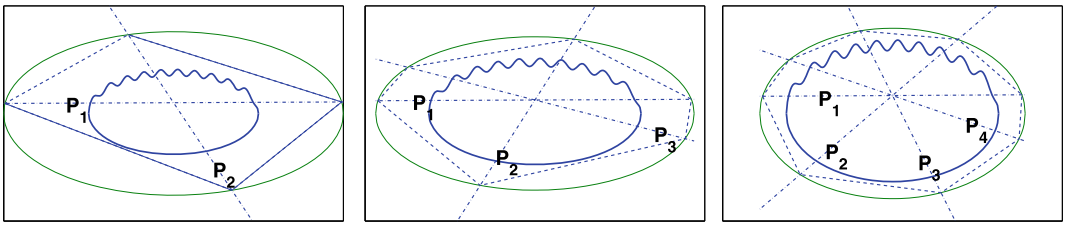

Fig. 16 Example illustrating minimum number of planes required for sectioning

perform the collision cone computations for guaranteed collision avoidance and having greater than two planes would be computationally wasteful. However, if we take a slightly tighter bounding ellipse (see Fig. 16(b)), then repeating the above procedure, we find that we need at least three planes P_1, P_2 and P_3. The tightest bounding ellipse considered (see Fig. 16(c)) would require at least four planes P_1, P_2, P_3 and P_4. Thus the smaller the bounding ellipse, the larger the number of planes required to get an approximate collision cone that is suitable for guaranteed collision avoidance. The minimum number of planes required is thus a function of both the arbitrary object as well as the size of the bounding quadric chosen. Finally, the avoidance maneuver can be generated on any of the chosen planes (say either P_1 or P_2 in case (a)), by applying the acceleration law (25) on that plane. If larger number of planes are available, then the choice can be optimized with respect to some objective function or a suitable plane can be chosen taking into account other obstacles in the vicinity.

7 Collision avoidance between two arbitrary objects moving in space

We finally address the question of generating approximations to the 3-D collision cone between two objects of arbitrary shape, moving in space. We first discuss the case when A and B are spheres, before the more general case when they are both of arbitrary shape.

Consider an engagement between two spheres A and B. If we construct a plane that contains $\vec{V}_A$ and $\vec{V}_B$ and also passes through both A and B, then we can restrict our consideration to only this (parallel set of) planes. Take any one plane from this set and consider the circular section C_1 (of sphere A) and C_2 (of sphere B) that lie on this plane. We can then say the following:

If C_1 is on a collision course with C_2, then A is also on a collision course with B. If C_1 is not on a collision course with C_2, then A is not on a collision course with B.

We can then state the following lemma:

Lemma 8 *Consider an engagement between two circular objects C_1 and C_2 of radius R_1 and R_2 moving with constant velocities such that $\vec{V}_{C1}$, $\vec{V}_{C2}$, C_1, C_2 all lie on a single plane $\mathcal{P}$ in space. Then C_1 is on a collision course with C_2 if and only if (17) is satisfied with $V_{\theta 0}$, $V_{\phi 0}$ and V_{r0} representing the relative velocity components of the line joining the centers of C_1 and C_2. Here, r_0 represents the distance between the centers of C_1 and C_2 and $R = R_1 + R_2$ in (17).*

Proof We can construct imaginary spheres $\mathcal{A}$ and $\mathcal{B}$ such that C_1 is a great circle of $\mathcal{A}$ and C_2 is a great circle of $\mathcal{B}$. The proof then follows from the above discussion. □

An important corollary of Lemma 8 is that by using the dynamic inversion based guidance law (25) with a (δ, γ) pair such that $\vec{V}_A$ remains on $\mathcal{P}$, A will avoid B.

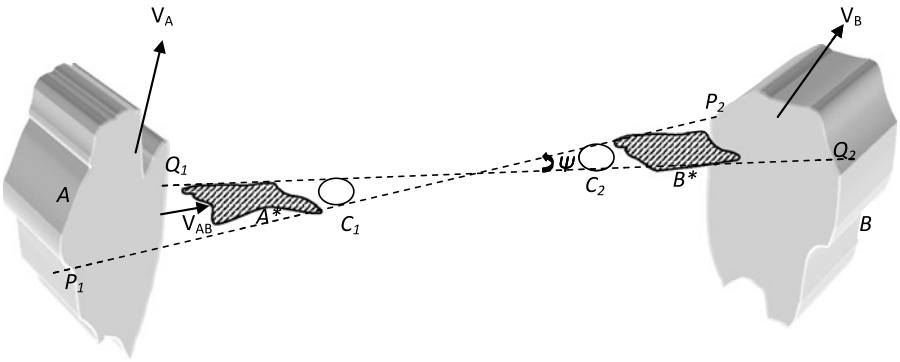

Fig. 17 Collision between two arbitrary objects

7.1 Planar section of exact collision cone

Refer to Fig. 17 which shows the collision geometry between two arbitrary objects A and B, which have constant velocities $\vec{V}_A$ and $\vec{V}_B$, respectively. Let $\vec{V}_{AB}$ denote the relative velocity vector. Now construct any arbitrary plane $\mathcal{P}$ that passes through both A and B and is parallel to $\vec{V}_{AB}$. Let A^* represent the intersection of $\mathcal{P}$ with the object A and B^* represent the intersection of $\mathcal{P}$ with the object B. The following cases then arise:

(a) If A^* and B^* are not both disjoint: Let P_1P_2 and Q_1Q_2 represent two lines that are tangents to A^* and B^*, constructed such that they form a planar section of a cone with A^* and B^* lying on opposite sides of the vertex of this cone. Let the vertex angle of this cone be ψ. Now we can always construct two imaginary circles C_1 and C_2 that lie on the same plane $\mathcal{P}$ and are tangential to P_1P_2 and Q_1Q_2. Then, from Lemma 8 A^* is on a collision course with B^* if and only if C_1 is on a collision course with C_2. It then follows that A^* is on a collision course with B^* if and only if (24) is satisfied.

(b) If A^* and/or B^* is disjoint (this can occur in situations where A and/or B is non-convex), then A^* is on a collision course with B^* if and only if (69) is satisfied for some part i, with ψ_i now representing the included angle of the sector formed by the ith pair of (intersecting) lines that are tangential to both A_i^* and B_i^*. Here, $V_{\theta 0i}$, $V_{\phi 0i}$ and V_{r0i}, are the relative velocity components of the angular bisector of this sector.

We point out that in case (a), (24) cannot be directly used to compute the collision cone between A^* and B^*. However, by taking the intersection of the plane $\mathcal{P}$ with the spatial cone generated by (24), we get an exact representation of the planar collision cone between A^* and B^*. This is obtained as shown in (71). A similar argument holds for case (b) as well. Finally, by using the acceleration law given in (25), an avoidance maneuver can be generated on that plane.

7.2 Approximation to spatial collision cone

While the preceding subsection demonstrates conditions that are both necessary and sufficient for collision between A^* and B^*, these conditions are only sufficient for collision between A and B. This is because there can be situations where A is on a collision course with B even though A^* is not on a collision course with B^*. However, the above results can be suitably used to generate approximations to the 3-D collision cone as follows.

Let A have m collision warning sensors $s_1, s_2, \ldots, s_m$ mounted on it at different locations. Consider the jth sensor. Shift the velocity vector $\vec{V}_B$ to the location of s_j and define a plane Ω_{1j} that passes through the location of s_j and contains $\vec{V}_B$. If Ω_{1j} passes through both A and B, then let B_{1j} represent the intersection of Ω_{1j} with B, and A_{1j} represent the intersection of Ω_{1j} with A. We can now construct the smallest planar cone such that A_{1j} and B_{1j} are each wholly contained on opposite sides of the cone. If ψ_{1j} denotes the vertex angle of this cone, then the results of the preceding subsection can be used to obtain a collision cone X_{1j}. Repeat this procedure for all the m sensors using m parallel planes $\Omega_{11}, \ldots, \Omega_{1m}$ and obtain the collision cones $X_{11}, \ldots, X_{1m}$ on these planes. The union of all these collision cones gives the collision cone X_1 on the plane Ω_1.

Next, rotate the plane Ω_1 about the $\vec{V}_B$ vector to obtain the plane Ω_2 and then repeat the procedure for all the m sensors. This is done for n such planes, so that we finally obtain n two-dimensional cones $X_1, \ldots, X_n$. The determination of what constitutes an adequate number of planes can be based upon the discussion in the previous section. These are then combined using the procedure given in the previous section to obtain the approximation to the complete 3-D collision cone between A and B.

Once the collision cone corresponding to each sensor for a given plane is obtained, the collision times can be computed. The minimum of these can be considered as the collision time associated with the planar cone. This computation can be repeated for each Ω plane and the minimum of all the collision times will be the collision time associated with

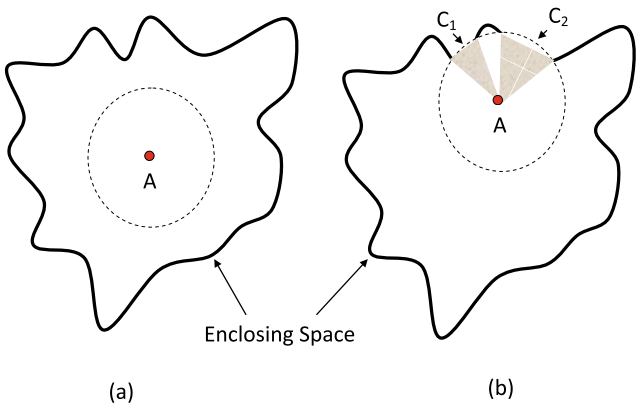

Fig. 18 Collision cones in closed environments. In (**a**), the safety circle lies completely inside the closed space whereas in (**b**), the safety circle intersects the boundaries of the closed space

the overall collision cone. Finally, by using the dynamic inversion based acceleration law (25), an avoidance maneuver can be computed on any chosen plane.

The quadric surface approximation of objects will produce collision cone approximations that contain the exact collision cone since the objects are represented by and contained in bounding boxes. This will lead to safe collision avoidance strategies. Computationally, the sectioning strategy leads to simpler and faster computations (per section), whereas the computation for the quadric surface based 3-D collision cone requires somewhat higher computational effort. However, note that to get a reasonably accurate approximation of the exact collision cone in 3-D, one needs to do the 2-D computations for a large number of planes, thus pushing up the computational cost. But the 3-D quadric surface based collision cone computation remains unchanged. Essentially, it shows that although simple, the logical extension of 2-D collision cone actually leads to higher computations if it has to be reasonably accurate, but the quadric surface based 3-D collision cone strategy is computationally less time taking and assures development of guaranteed collision avoidance strategies while also precluding the necessity of using overly conservative spherical bounding boxes. This aspect is crucial to the justification of using quadric surface based 3-D collision cones for developing collision avoidance strategies.

8 Some special cases

In this section, we address some special cases that are of great importance for a full-fledged implementation of a collision cone based avoidance strategy. We indicate methods by which collision-free trajectories can be generated in closed spaces and in the presence of multiple obstacles using the basic quadric surfaces collision cones and avoidance strategies coupled with the notion of time-to-collision. For lack of space, we give only the fundamental concepts underlying these methods here, but these are sufficient to make an implementation of the collision cone based avoidance strategy possible.

8.1 Collision avoidance in closed spaces

When an object A moves inside a closed space then, due to sensor reflections from the walls of the closed space, A would infer that it is always inside a collision cone regardless of which direction it moves. We propose a strategy that works well in general, but is well-suited for the specific cases where the object is in a closed space. The determination of the time to collision $t_{m,k}$ plays a crucial role in this strategy. The time to collision $t_{m,k}$ to any obstacle can be computed using (16) (with '0' replaced by 'k' in the subscript). Object A then ignores a collision cone if the $t_{m,k}$ associated with that cone is larger than a pre-defined safety threshold and treats this space as being free-space. An illustration is given in Fig 18, which shows A navigating in a closed space. The safety circle is shown in dashed lines and its radius is based on the safety threshold. In Fig. 18(a), this safety circle lies completely inside the enclosure and therefore A can fully ignore the 360° collision cone generated by the walls of the enclosure. In Fig 18(b), the safety circle intersects the walls of the enclosure and A uses these points of intersection to generate two collision cones C_1 and C_2, which can then be avoided using the acceleration laws discussed in the earlier sections. This strategy is general enough to be applied in any situation, irrespective of if it is a closed space or not. In fact, we will now extend this idea to handle multiple obstacles as well.

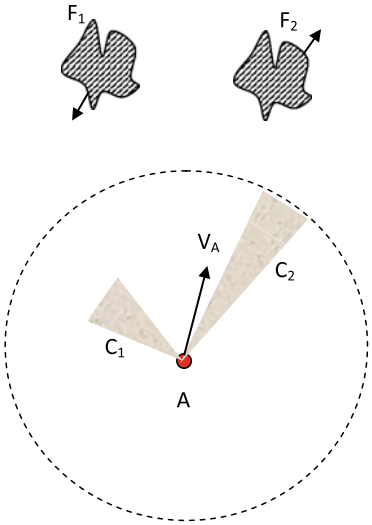

Fig. 19 Choosing a path between two collision cones C_1 and C_2 that are of unequal lengths

8.2 Collision avoidance for multiple obstacles

When an object A has to navigate in an environment with multiple obstacles, the collision cone to each obstacle is interpreted as a cone of finite length with the length of the cone being proportional to the time to collision with that obstacle. This way the different collision cones are prioritized based on the $t_{m,k}$ or $t_{go,k}$ (obtained from (16) and (29)) associated with each obstacle. Note that this idea is not much different from what was proposed for closed spaces, only that it quantifies the "risk" associated with an obstacle as a function of the time of collision. A representative example is given in Fig. 19, which shows A having to avoid two identical obstacles F_1 and F_2, that are initially equidistant from A, with C_1 and C_2 being their respective collision cones. Assume that $\vec{V}_A$ lies outside both C_1 and C_2. Now if t_{go} associated with both C_1 and C_2 are identical, then we interpret both C_1 and C_2 as having identical risk factors as the collision cones are of equal lengths. It would be logical to maneuver so that $\vec{V}_A$ would have a heading that lies midway between the boundaries of C_1 and C_2. Such a path is generated by using identical (positive) values of the reference signal $v(t)$ and/or the gain K in the dynamic-inversion based avoidance maneuvers presented in previous sections. On the other hand, if t_{go} associated with F_1 is smaller than that associated with F_2, then we interpret C_1 as having a shorter length than C_2 (as shown in the figure). Then, since there is a higher risk factor associated with C_1, A can take a path that is initially farther away from C_1 than C_2. Such a path is generated by using different values of the reference signal $v(t)$ and/or K for F_1 and F_2, with these values being chosen in the ratio of their respective t_{go} values. A schematic is provided in Fig. 20, wherein the choice of the collision cones $C_1, \ldots, C_q$ has to be done judiciously. It should contain only those collision cones which are in the near vicinity of the $\vec{V}_A$. It is noted that such an approach would correspond to an efficient integration of the collision cone equations with a weighted Voronoi-based approach (Guruprasad and Ghose 2008). Trajectory deformation schemes (Fraichard and Delsart 2009) can also be integrated with the collision cone approach. Even a potential fields approach, where the less risky cone (or the longer cone) produces a lower repulsive force than the more risky cone (shorter cone), can be applied to handle this problem. In fact, there has been some work in the literature (Ferrara and Rubagotti 2007) that integrates the 2-D collision cone equations of Chakravarthy and Ghose (1998) with a potential function based approach. Such ideas hold similar promise with the 3-D collision cone equations, as well.

The velocity obstacle literature (Shiller et al. 2010) introduces the notion of a fixed time-horizon in a sense different from this paper, to deal with closed spaces by determining a threshold velocity for collision. Finally, note that although we have treated the above two cases separately for clarity, the use of the time-to-collision to categorize collision cones and use them for collision avoidance is an idea that is universally applicable in all situations including multiple obstacles and closed spaces.

The collision cones and the various guidance laws presented in the paper come with certain guarantees with which they are effective in a single obstacle scenario. These avoidance maneuvers also lay a solid platform to work with in scenarios of multiple obstacles. Determination of guarantees that can be provided on collision avoidance in multi-obstacle scenarios, however remains an open area of research.

9 Conclusions

In this paper, we address the problem of guaranteeing safe trajectories between objects moving in a three dimensional environment. We consider objects whose shapes (or their projections on a plane) can be modeled by quadric surfaces, which is a class of surfaces that includes not just spheres, but also ellipsoids and hyperboloids. While a sphere represents a standard bounding box approximation that is commonly used in the literature, there can be many objects for which an ellipsoid can serve as a better approximation and there are many other non-convex objects for which a hyperboloid-like shape can serve as a good approximation. We use the collision cone approach, previously developed in Chakravarthy and Ghose (1998), to demonstrate exact analytical expressions for collision cones of such quadric surfaces. These are subsequently used to develop acceleration laws for collision avoidance of the quadric surfaces. For arbitrarily shaped objects, a procedure is developed that combines exact representations of 2-D collision cones on multiple planes into an

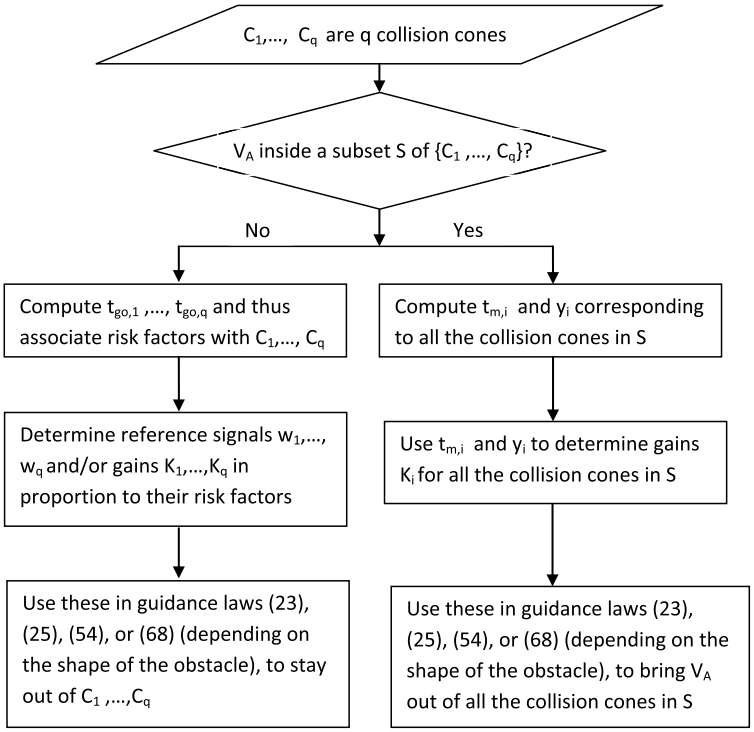

Fig. 20 Flowchart denoting use of avoidance laws in multi-obstacle scenario

approximate 3-D collision cone, and the associated avoidance maneuvers are discussed. Future work could include determination of optimal avoidance maneuvers in a multi-obstacle scenario.

References

Belkouche, F. (2009). Reactive path planning in a dynamic environment. *IEEE Transactions on Robotics, 25*(4).

Belkouche, F., & Belkouche, B. (2008). Kinematics-based characterization of the collision course. *International Journal of Robotics and Automation, 23*(2).

Bendjilali, K., & Belkhouche, F. (2009). Collision course by transformation of coordinates and plane decomposition. *Robotica*.

Carbone, C., Ciniglio, U., Corraro, F., & Luongo, S. (2006). A novel 3-D geometric algorithm for aircraft autonomous collision avoidance. In *Proc. of the 45th IEEE conference on decision and control* (pp. 1580–1585). San Diego, CA, USA, December 2006.

Chakravarthy, A., & Ghose, D. (1996). Capturability of realistic generalized true proportional navigation. *IEEE Transactions on Aerospace and Electronic Systems*, *32*(1), 407–417.

Chakravarthy, A., & Ghose, D. (1998). Obstacle avoidance in a dynamic environment: a collision cone approach. *IEEE Transactions on Systems, Man and Cybernetics. Part A. Systems and Humans*, *28*(5), 562–574.

Chakravarthy, A., & Ghose, D. (2011). Collision cones for quadric surfaces. *IEEE Transactions on Robotics, 27*(6).

Choi, Y.-K., Wang, W., Liu, Y., & Kim, M.-S. (2006). Continuous collision detection for two moving elliptic disks. *IEEE Transactions on Robotics*, *22*(2), 213–224.

Choi, Y.-K., Chang, J.-W., Wang, W., Kim, M.-S., & Elber, G. (2009). Continuous collision detection for ellipsoids. *IEEE Transactions on Visualization and Computer Graphics*, *15*(2), 311–324.

Ferrara, A., & Paderno, J. (2006). Application of switching control for automatic pre-crash collision avoidance in cars. *Nonlinear Dynamics*, *46*, 307–321.

Ferrara, A., & Rubagotti, M. (2007). Sliding mode control of a mobile robot for dynamic obstacle avoidance based on a time-varying harmonic potential field. In *ICRA 2007 workshop on planning, perception and navigation for intelligent vehicles*, Roma, Italy, 2007.

Ferrara, A., & Vecchio, C. (2007). Collision avoidance strategies and co-ordinated control of passenger vehicles. *Nonlinear Dynamics*, *49*, 475–492.

Ferrara, A., & Vecchio, C. (2009). Second order sliding mode control of vehicles with distributed collision avoidance capabilities. *Mechatronics*, *19*, 471–477.

Fiorini, P., & Shiller, Z. (1998). Motion planning in dynamic environments using velocity obstacles. *The International Journal of Robotics Research*, 17.

Fraichard, T., & Delsart, V. (2009). Navigating dynamic environments with trajectory deformation. *Journal of Computing and Information Technology, 17*(1).

Frazzoli, E., Mao, Z. H., Oh, J. H., & Feron, E. (2001). Aircraft conflict resolution via semi-definite programming. *Journal of Guidance, Control, and Dynamics*, *24*(1), 79–86.

Goerzen, C., Kong, Z., & Mettler, B. (2010). A survey of motion planning algorithms from the perspective of autonomous UAV guidance. *Journal of Intelligent & Robotic Systems*, *57*, 65–100.

Gross, J., Rajvanshi, R., & Subbarao, K. (2004). Aircraft collision detection and resolution using mixed geometric and collision cone approaches. In *Proc. of AIAA guidance, navigation and control conference*, Rhode Island, Providence, USA. Paper No. AIAA 2004-4879.

Guelman, M. (1976). The closed form solution of true proportional navigation. *IEEE Transactions on Aerospace and Electronic Systems*, *AES-12*(4), 472–482.

Guruprasad, K. R., & Ghose, D. (2008). Heterogeneous sensor based Voronoi decomposition for spatially distributed limited range locational optimization. In D.-S. Kim & K. Sugihara (Eds.),

Voronoi's impact on modern science, Book 4: Vol. 2. Proceedings of 5th annual international symposium on Voronoi diagrams (ISVD 2008) (pp. 78–87). Kiev, Ukraine, September 2008.
Hilbert, D., & Cohn-Vossen, S. (1952). *Geometry and the imagination*. New York: Chelsea.
Ju, M.-Y., Liu, J.-S., Shiang, S.-P., Chien, Y.-R., Hwang, K.-S., & Lee, W. C. (2001). A novel collision detection method based on enclosed ellipsoid. In *Proc. of the 2001 IEEE international conference on robotics and automation* (pp. 2897–2901). Seoul, Korea.
Khatib, O. (1986). Real-time obstacle avoidance for manipulators and mobile robots. *International Journal of Robotics Research, 5*(1).
Kim, C., Haas, C. T., Liapi, K. A., & Caldas, C. H. (2006). Human-assisted obstacle avoidance system using 3D workspace modeling for construction equipment operation. *Journal of Computing in Civil Engineering*, 177–186.
Lalish, E., & Morgansen, K. A. (2008). Decentralized reactive collision avoidance for multi-vehicle systems. In *Proc. of 47th IEEE conference on decision and control*, Cancun, Mexico, December 2008.
Large, F., Laugier, C., & Shiller, Z. (2005). Navigation among moving obstacles using the NLVO: principles and applications to intelligent vehicles. *Autonomous Robots*, *19*, 159–171.
Lin, C. (1991). *Modern navigation, guidance and control processing*. Englewood Cliffs: Prentice Hall.
Lozano-Perez, T. (1983). Spatial planning: A configuration space approach. *IEEE Transactions on Computing, C-32*.
Shiller, Z., Large, F., & Sekhavat, S. (2001). Motion planning in dynamic environments: obstacles moving along arbitrary trajectories. In *Proc. of the 2001 IEEE international conference on robotics and automation*, Seoul, Korea.
Shiller, Z., Gal, O., & Fraichard, T. (2010). The nonlinear velocity obstacle revisited: The optimal time horizon, Workshop on guaranteeing safe navigation in dynamic environments. In *IEEE international conference on robotics and automation*, May 2010.
Shneydor, N. A. (1998). *Missile guidance and pursuit: kinematics, dynamics, and control*. Horwood: Chichester.
Slotine, J., & Li, W. (1991). *Applied nonlinear control*. New York: Prentice Hall.
Tyan, F. (2005). Unified approach to missile guidance laws: a 3D extension. *IEEE Transactions on Aerospace and Electronic Systems, 41*(4).
Watanabe, Y., Calise, A. J., Johnson, E. N., & Evers, J. H. (2006a). Minimum-effort guidance for vision-based collision avoidance. In *Proc. of AIAA atmospheric flight mechanics conference*, Keystone, Colorado, USA, August 2006. Paper No. AIAA 2006-6641.
Watanabe, Y., Johnson, E. N., & Calise, A. J. (2006b). Vision-based guidance design from sensor trajectory optimization. In *Proc. of AIAA atmospheric flight mechanics conference*, Keystone, Colorado, USA. August 2006. Paper No. AIAA 2006-6607.
Watanabe, Y., Calise, A. J., & Johnson, E. N. (2007a). Vision-based obstacle avoidance for UAVs. In *Proc. of AIAA guidance, navigation and control*, Hilton Head, South Carolina, USA, August 2007. AIAA 2007-6829.
Watanabe, Y., Johnson, E. N., & Calise, A. J. (2007). Stochastically optimized monocular vision-based guidance design. In *Proc. of AIAA atmospheric flight mechanics conference*, Hilton Head, South Carolina, USA, August 2007. Paper No. AIAA 2007-6865.
Zarchan, P. (1990). *Tactical and strategic missile guidance*. Washington: AIAA.

Animesh Chakravarthy is an Assistant Professor with a joint appointment in the Departments of Aerospace Engineering and Electrical Engineering at Wichita State University. He obtained his Master's Degree in Aerospace Engineering at the Indian Institute of Science, in 1994; and his Ph.D. in the Department of Aeronautics and Astronautics at the Massachusetts Institute of Technology in 2007, with specialization in Estimation and Control. During 1994–2001, he was a Scientist/Engineer at the Aeronautical Development Agency, India in the Flight Mechanics and Control Division and during 2007–2010, he was a Research Scientist at the University of Florida Research and Engineering Education Facility. He has been a faculty at Wichita State University since 2011. His research interests include dynamics and control of morphing vehicles, path planning in dynamic environments, multi-vehicle systems and study of insect flight dynamics.

Debasish Ghose received the B.S. degree from the Regional Engineering College, Rourkela, India (presently a National Institute of Technology), in 1982, and the M.S. and Ph.D. degrees from the Indian Institute of Science, Bangalore, India, in 1984 and 1990, respectively. He is a Professor with the Department of Aerospace Engineering, Indian Institute of Science, Bangalore, and heads the Guidance, Control and Decision Systems Laboratory and the Mobile Robotics Laboratory. His main research interests are in the area of guidance and control of unmanned aerospace vehicles, robots, and other multiagent systems. In the past, he has been a visiting faculty in several universities including the University of California at Los Angeles and lectured at several international conferences and workshops. Prof. Ghose is on the editorial board of many international journals including the IEEE Transactions on Systems, Man, and Cybernetics, the IEEE Transactions on Automation Science and Engineering, IEEE Transactions on Aerospace and Electronic Systems, and the Proceedings of IMechE (U.K.). He is a Fellow of the Indian National Academy of Engineering.